Chapter 1

Powder Characterization and Testing

Oleg D. Neikov, Dina V. Lotsko, Frantsevich Institute for Problems of Materials Science (IPMS), Kiev, Ukraine
Victor G. Gopienko, Russian National Aluminium-Magnesium Institute (VAMI), St. Petersburg, Russia

Apparent density, tap density, angle of repose, flow rate, compressibility and green strength are referred to as the physical–technological properties of powders. These properties, for a certain powder composition, may depend on its granulometric composition, particle shape, particle morphology, specific surface, moisture content, etc. Knowledge of technological parameters coupled with the physical properties enables evaluation of the behavior of powder during processing that is accomplished by their consolidation. The procedures described in standards are used to determine the technological properties of powders in delivery condition.

To evaluate powder properties the standard monitoring methods are used. The standard demands of the ISO are the base for the development of regional, national and branch standards. Usually, in contrast to ISO, a feature of these standards is the fact that they contain additional or refined specifications. Appendix 1 at the end of the book contains the list of the standard methods of powder characterization and testing.

Obtaining reliable powder samples is of vital importance for getting genuine data of chemical composition and the physical and technological properties of a given powder. To obtain a representative powder sample for analysis, it is necessary to follow the principles of sampling described below.

Sampling of Powders

Sampling arrangement and the subsequent partition of the selected samples that are needed for tests are laid down in ISO 3954. An analogous standard functions in North America (ASTM Standard B215) and in the USA (MPIF Standard 01).

Generally, two methods are used for obtaining samples of metal powders for subsequent testing. The first method is provided for sample take-off while the powder is in motion. A general rule in this method is that the whole of the stream of powder should be taken for many short increments of time, in preference to a single part of the stream being taken. This may be done when blenders or storage tanks are being emptied by screw or belt conveyors.

In the standard, the following sample types, represented in the sampling scheme in Figure 1.1, are distinguished. In the standard, the following terms are defined:

- lot – a definite quantity of powder processed or produced under uniform conditions
- increment – a quantity of powder obtained by a sampling device at one time from a single lot
- gross sample – a quantity of powder, adequate for the tests to be performed, consisting of all of the increments taken from a single lot
- composite sample – the blended entire gross sample
- test sample – a quantity of powder taken from the composite sample for determination of a single property or for preparing test pieces. It should normally be taken by splitting the composite sample
- test portion – a defined quantity of powder drawn from the test sample, on which the test is performed or from which test pieces are produced.

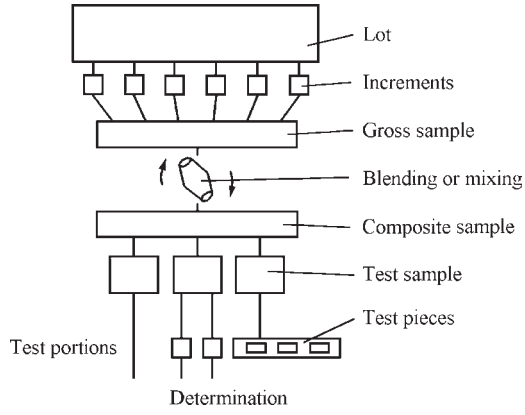

Figure 1.1 Sampling scheme.

Table 1.1 Recommended number of containers to be selected from a packaged lot

Number of containers in lot	Number of containers to be selected
1–5	All
6–11	5
12–20	6
21–35	7
36–60	8
61–99	9
100–149	10
150–199	11
200–299	12
300–399	13
More than 400	13 + 1 per 100 additional containers

At least three increments shall be taken for each lot of powder. The actual number depends on the size of the lot and the powder involved and shall be agreed upon by the parties involved.

The second method is used for sampling stored non-flowing materials: powders already packaged in containers. They may be stored in small containers such as drums or bags, or in large containers such as trucks or railway wagons. Several of these containers should be selected systematically or, preferably, using a table of random numbers. The standard recommends the number of samples depending on the total number of containers (Table 1.1). Sampling accuracy is provided by means of a sampling spear. The MPIF Standard 01 recommends the use of the keystone sampler, consisting of two coaxial tubes, outer and inner, closed from the bottom and with windows in the sides. The bottom part of the sampler is provided with a screw and from above is supplied by a handle. In the closed position, the sampler is inserted into the powder at a point 70% of the distance from the center of the cross-section to the periphery and straight down to the bottom of the container. The sampler is twisted to the open position, allowing powder to flow into the sampler tube. After filling, the sampler tube is closed and the sampler is removed from the container.

In sampling from trucks and wagons, it is recommended that eight samples be extracted [1]. No increment should be taken less than 300 mm below the surface in order to avoid sampling from the surface layer in which segregation can occur due to vibration (Figure 1.2).

The gross sample is often too large to be handled easily and may have to be reduced to a more opportune weight. Several methods are used for sample reduction.

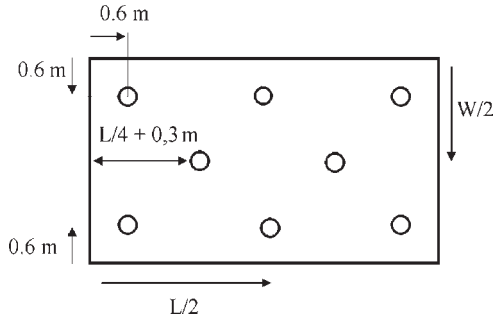

Figure 1.2 Sampling points for a truck or a wagon.

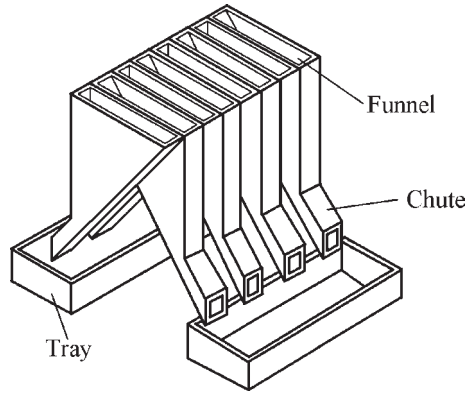

Figure 1.3 Sample splitter.

- *Scoop sampling* consists of plunging a scoop into the powder and selecting a sample. Such samples may not be representative of the bulk because the sample is taken from the surface and the sampling device does not pass through the whole heap.
- *Conical pouring and quartering* consists of pouring the powder into a heap on a flat horizontal surface and dividing by a cross-shaped cutter. The powder from two opposite portions is integrated in the common sample that in turn is divided into four parts for subsequent testing.
- *Chute splitting* is adopted for sample division. The chute splitter consists of funnels located along the bottom and forming two lines of chutes that separately feed two trays placed on either side of the chute (Figure 1.3).

All above methods are simple and therefore popular owing to the fact that samplers contain no moving parts and are inexpensive.

- A *rotary sample divider* for free-flowing powders is shown in Figure 1.4. Several versions of this device were designed for dusty powders, and some for cohesive powders.

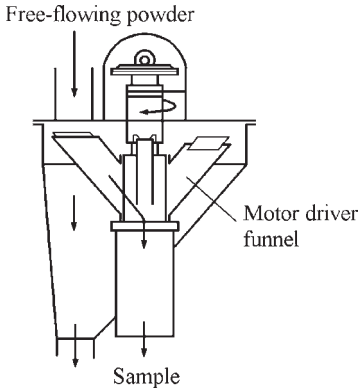

Figure 1.4 Rotary sample divider.

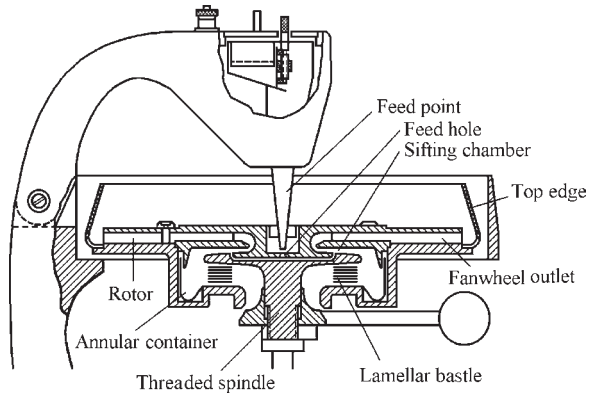

Figure 1.5 Simplified schematic draft of the Bahco classifier.

The reliability of selected methods was examined using binary mixtures of coarse and fine sand (60:40 ratio). It was deduced that the standard deviations amounted to 6.81 and 5.14%, respectively, for quartering and scoop sampling methods. Consequently, little confidence can take place in the first two techniques. For the chute splitting method and rotary sample divider, the standard deviations amount to 1.01 and 0.146%, respectively. Hence, the rotary sample divider is better than all the other methods.

Weight of Sample

The limiting (minimum) weight of the gross sample may be calculated using the following simple formula:

$$M_s = \frac{1}{2}\left(\frac{\rho}{\sigma_i^2}\right)\left(\frac{1}{w_1} - 2\right)d_1^3 \times 10^3 \qquad (1)$$

where M_s is the limiting weight in grams, ρ is the powder density in g/m^3, σ_i^2 is the variance of the tolerated sample error, w_1 is the fractional mass of the coarsest size class being sampled and d_1^3 is the arithmetic mean of the cubes of the extreme diameter in the size class in cubic centimeters. This equation is applicable when the coarsest class covers a size range of not more than 1.41:1 and w_1 is less than 50% of the total sample.

ISO 3081 recommends a minimum incremental mass depending on the maximum particle size in millimeters. According to this standard, the minimum mass of increment with maximum particle size of 10–0 mm amounts to 0.3 kg.

Particle Size Distribution Analysis

The classification process is used to determine particle size distribution or to separate certain particle sizes from a distribution. Generally, powder classification is based on the movement of the suspended particles in a fluid, under the action of a force field which is created by gravity, centrifugal or coriolis, and inertia forces. The fluid is usually air or water. The classifiers may be distinguished depending on the stream direction: counterflow equilibrium and cross-flow separation. The classifiers such as elutriators, zigzag classifiers, and Bahco centrifugal classifier, are related to the counterflow equilibrium devices [2]. The Bahco classifier (Figure 1.5) can be graded in the size range from 5 to 100 μm. For the samples, 5–10 g of powder are required.

Sieve Analysis

Sieve analysis is the method most widely used in the PM industry for determination of particle size distribution of metal powders larger 5 μm. Wire cloth sieves woven in a square mesh pattern of phosphor bronze or stainless steel are mounted in 75 or 200 mm stainless steel or brass rings. A series of sieves is selected that covers the full range of particle sizes present in a given powder. The sieving unit with sieve series, where sieves are stacked in order, with the largest mesh size at the top and a pan at the bottom, on a shaker with rotary and tapping action, is shown in Figure 1.6.

Test sieves according to the international and national standards are represented in Table 1.2. The standard sieve series are specified in ISO standards 565 and 3310/1, ASTM standard E 11 and CIS standard GOST 3584.

ISO sieve series is based on the principle of a fixed ratio between the sieve openings with selection of the row of preferable numbers: with the denominator of $\sqrt[20]{10} \approx 1.12$ (R 20) for supplementary sizes and selection of each third number from row numbers for principal sizes (R 20/3 ≈ 1.4).

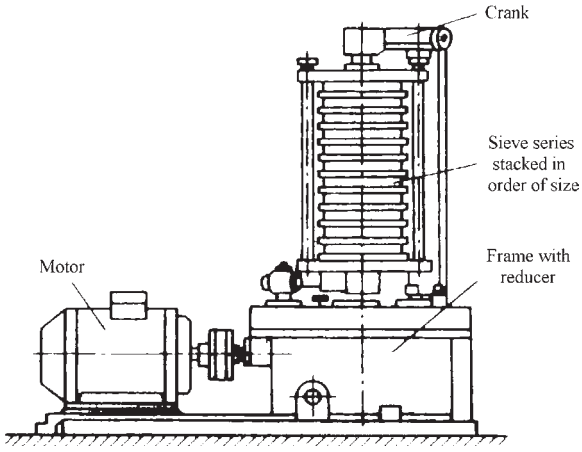

Figure 1.6 Sieving classifier.

The process for carrying out the sieve analysis of metal powders is laid down in ISO 4497. Analogous standards are used in North America (ASTM Standard B 214), in CIS (GOST 18318–94) and in the USA (MPIF Standard 05).

The main sieving problems are as follows. In the case of an overloaded sieve, the weight of the oversized powder tends to wedge the near-mesh particles into the openings or near-mesh oversized particles become entrapped in the openings. If brushing fails to remove the particles, an ultrasonic wash with a wetting agent must be used to eliminate them. Typically, the irregularly shaped particles are able to pass through sieve openings in a certain orientation only. Usually vibrating and shaking are sufficient to change the orientation of particles.

Damaged sieves may have stretched and distorted the mesh openings or may be torn. A microscope should be used to examine sieves regularly. Epoxy has been used to repair small damages.

Electrostatic charges may cause fine particles adhere to each other, forming an agglomerate of particles. Fine particles also can adhere to larger particles. The use of sieving aids, such as commercial antistatic agents, may lessen the agglomeration.

Micromesh sieves have the advantage in comparison with wire cloth sieves but they are more expensive. The micromesh sieves are manufactured by photo-etching and electrodeposition techniques. This method makes it possible to produce flat sheets of electrodeposited nickel with precise square openings. This thin gauze is supported by a coarser square-etched grid of nickel-plated cupronickel. ASTM E 11-87 specification claims a maximum deviation of only $\pm 2.0\,\mu m$ for sieves ranging from 125 to 5 μm.

Irrespective of sieve types, for sieves finer than 45 μm (325 mesh) most dry sieving techniques are deficient. For these finer size sieves, a jet type siever can

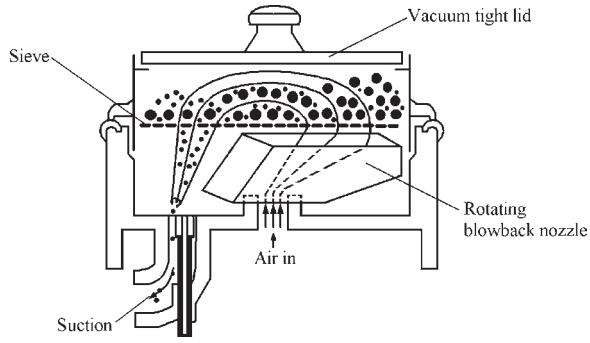

Figure 1.7 Micromesh jet sieve.

be used, such as the Alpine production (Figure 1.7). This device uses an exhaust coupled with a rotating blowback nozzle. Fine particles are suctioned through the mesh, while the blowback nozzle redistributes the powder sample on the sieve, thus disintegrating agglomerates and purging the mesh openings. The sieving operation is rapid and permits sieving down to 10 μm.

Sieves are installed consistently; sieves with the larger apertures are placed above. A set of sieves is placed on a vibrating table. The top sieve is filled with a powder shot of 100–300 g. Sieving is carried out for 15–20 min, then the residue on each sieve is weighed and the percentage of this fraction is determined. More information on analysis procedures can be found in the ASTM edition [3].

In Table 1.8 a list of the devices for determination of the granulometric structure of metal powders is given.

Sedimentation Methods

Sedimentation methods are based on the classifying of metal powders depending on the settling rate under gravity of particles situated in a fluid. This determination is based on Stokes's law of fluid dynamics by laminar current. That states that the frictional force, F_r on a spherical particle moving through a fluid at constant velocity is proportional to the product of constant velocity, the fluid velocity, ν, the fluid viscosity η and the radius of the sphere, r:

$$F_r = -6\pi\eta r\nu \tag{2}$$

Measuring this velocity, ν_{st}, it is possible, with the help of Stokes' equation, to determine the radius, r, of settling particles:

$$r = \sqrt{\frac{9\eta\nu_{st}}{2g(\rho_s - \rho_f)}} \tag{3}$$

Table 1.2 Standard sieve series

ISO 565 and 3310/1		DIN 4178	ASTM E 11	CIS GOST 3584	British Standard	
Principal sizes (R 20/3)	Supplementary sizes (R 20)				Sieve designation	
μm	μm	μm	μm	mm	μm	mesh
1000[a]	1000[a]	1000[a]	1000[a]	1.00	1000	16
	900	900				
	800	800	850	0.80	850	18
710	710	710	710		710	22
	630	630		0.63		
	560	560	600		600	25
500	500	500	500	0.50	500	30
	450	450				
	400	400	425	0.40	425	36
355	355	355	355		355	44
	315	315		0.315		
	280	280	300		300	52
250	250	250	250	0.250	250	60
	224	224				
	200	200	212	0.200	212	70
180	180	180	180		180	85
	160	160		0.160		
	140	140	150		150	100
125	125	125	125	0.125	125	120
	112	112				
	100	100	106	0.100		
90	90	90	90	0.090	90	170
	80	80		0.080		
	71	71	75	0.071	75	200
63	63	63	63	0.063	63	240
	56			0.056		
	50	50	53	0.050	53	300
45	45	45	45	0.045	45	350
	40	40		0.040		
	36	36	38		38	400
	32	32	32			
	28	28				
	25	25	25			
	22	22				
	20	20				

[a] The beginning of sieve series is 125 mm. The range up to 1000 μm is not presented here.

where ρ_s is solid density, ρ_f is fluid density and g is gravitational acceleration.

To ensure accurate results, convection currents must be eliminated in the suspending fluid and the relative rate of motion between the fluid and powder particles must be slow enough to guarantee laminar flow. Usually this technique is used for the subsieve size range. These methods are applicable for sedimentation in air with limitation to particles larger 5 μm and, in liquids, particle sizes down to 0.1 μm can be determined. As particles size decreases, this method becomes unreliable because of the Brownian motion of the particles. The upper limit is 100 μm. Particles of more than 100 μm cause the display of medium inertia forces, which are not taken into account by Stokes' equation. The method is not suitable if particle shape strongly differs from spherical, for powders which cannot be dispersed or for agglomerated powders.

The suspension must be dilute enough to ensure independent motion to the maximum particle concentration even to 1 vol% of particles in the suspension. Compositions of dispersion liquids used for sedimentation analysis are given in Table 1.3.

Table 1.3 Liquids for preparation of suspensions

Powder	Liquid for suspension	Dispersion stabilizer
Aluminum	Water with pH value amount 3–4; Cy, Cye, Isopropanole, and Vegetable oil	ST of 0.1 wt%; Sfa OII-7 of 0.075 g/L
Boron carbide	WD; Butanol/ethanol	SP of 0.5 g/L
Bronze	Cy, Cye	SP of 0.5 g/L
Chromium	WD, Butanol, Kerosene	SPP of 0.001–0.002 mole/L
Cobalt	EA, n-Butanol, Isobutane	SP of 0.5 g/L
Copper	WD, Ethanol, Acetone, Cyl, n-Butanol, Isoamyl, EA, Water/glycerin in ratio 1:1	SP of 0.5 g/L
Lead	Cy, Cye, Acetone, n-Butanol	SP of 0.5 g/L
Magnesium	EA, n-Butanol	SP of 0.5 g/L
Manganese	Cye, Isobutanole	SP of 0.5 g/L
Molybdenum	EA, Acetone, WD, Water/glycerin, Water/glycol	Sodium hexametaphosphate of 0.1 g/L
Nickel	Water/glycerin, EA, n-Butanol/acetone, Cye	Alkyl polysulphonate of 0.1 g/L
Silver	Water/glycerin, EA	. . .
Tantalum	Cy, Cye	. . .
Tin	WD, n Butanol, Isobutanole	Alkyl sulphonate of 0.1 g/L
Titanium	WD, Cye	SSP of 0.5 g/L
Tungsten	WD, Water/glycerin, Ethanol, n-Butanol	Alkyl polysulphonate of 0.1 g/L Sodium hexamethophosphate of 0.1 g/L
Tungsten carbide	Water/glycerin WD	Sodium polyphosphate Alkyl polysulphonate
Zinc	Kerosene, EA, Cy, Butanol	. . .
Zirconium	Isobutanole, Methanol	Hydrochloric acid 0.01 g/L

Abbreviations: WD: water distillate; Cy: cyclohexanol; Cye: cyclohexanone; EA: ethyl alcohol; NS: naphtha soap; SC: sodium carbonate; Sfa: surfactant; SPP: sodium pyrophosfate ($Na_4P_2O_7$•$10H_2O$); SP: sodium phosphate (Na_3PO_4); ST: sodium tartrate

Among the number of sedimentation methods available, only a few are usually used for metal powders. Devices based on the method of accumulation of the deposition from the suspension that were popular in former times find an application at present too. Turbidimetry methods are widely used to determine the particle size distribution of refractory metal powders, such as tungsten and molybdenum. The micromerographs find a use to determine the particle size of subsieve metal powders.

Accumulation of the Sediment

The method of accumulating the deposit from a suspension consists of calculating the cumulative weight of powder settled from the fixed high suspension column h as a function of time. Construction of a curve of distribution function is shown in Figure 1.8. In the initial period, the increment sediment mass m is a linear function of the time τ.

$$m = k\tau$$

where k is the proportion coefficient or corner line coefficient (tangent of corner α_1, see Figure 1.8).

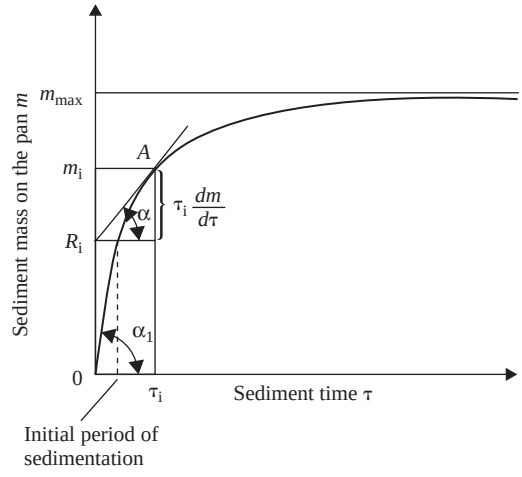

Figure 1.8 Construction of a curve of distribution function.

On completion of the initial period, the increment sediment mass on the pan starts to diminish, since all particles of the largest size have by then settled from the suspension. The increment sediment mass on the pan will continue to slow down as the sedimentation

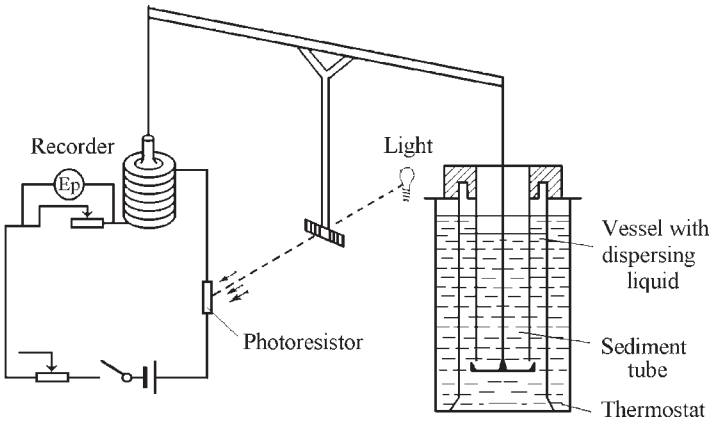

Figure 1.9 Liquid sedimentograph.

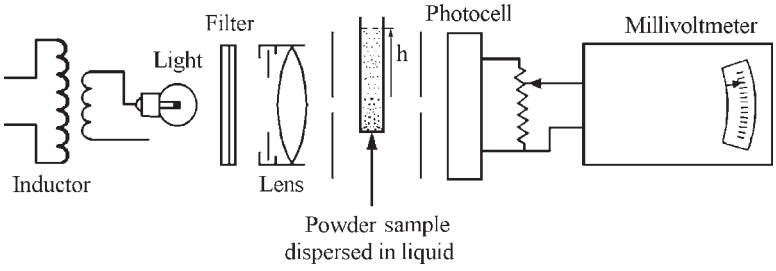

Figure 1.10 Schematic diagram of light turbidimeter.

of the particles of fixed sizes is completed. The function of sediment accumulation $m = f(\tau)$ in this period is graphically described by a smooth curve asymptotically approaching the straight line; m_{max} represents the maximum of mass sediment that can accumulate on the pan. The increment rate of the sediment $dm/d\tau$ constitutes the angle of slope of the tangent to the curve of sediment accumulation at the point corresponding to the time τ.

Since the sediment mass on the pan at the time τ_i (see Figure 1.8) is depicted by the segment projection on the ordinate line $A\tau_i$ (of the length $0m_i$) the tangent traced to this point of the curve divides this projection into two parts: a segment m_iR_i equal to τ_i $(dm/d\tau)$ that represents the mass of particles for which the settling rate is not higher than h/τ_i, and a segment $0R_i$, that constitutes the mass of particles for which the settling rate is not lower than h/τ_i, and therefore completely settled from the suspension in the column h at time τ_i. Accordingly, the ratio of $0R_i$ to $0m_{max}$ represents the fraction of particles, which have completely settled from the suspension.

Figure 1.9 shows a schematic diagram of a typical device based on the method of accumulation of the sediment from a suspension.

One serious disadvantage of the gravitational sedimentation techniques is the excessively long precipitation time for particles smaller than 5 μm. The centrifuging process can greatly accelerate the rate of settling [1].

Micromerographs

The micromerograph method consists of the accumulation of the sediment from the air of a suspended powder. A typical micromerograph includes a sediment chamber in the form of a vertical aluminum tube with an inside diameter of 10 cm and a height of 2.5 m. The pan, located at the bottom of the chamber, receives the sediment weight. Particle size distribution, being the first derivative of the function of sediment accumulation, is calculated on the basis of the obtained function $m = f(\tau)$ (see Figure 1.8) and Eqn 3. This device allows the determination of particle size distribution over the range 2 to 100 μm.

Turbidimetry

The turbidimeter is standardized in ASTM B 430. Figure 1.10 shows a schematic diagram of a typical

light turbidimeter. A sample of powder dispersed in a liquid is filled into a glass cell. A collimated beam of light passes through the cell at a level of a certain height of the vertical suspension column, h. The intensity of the light beam is determined by the current generated in a photocell and is measured by a recording millivoltmeter. The determination of the particle size distribution is based on the effect of attenuation of the light beam intensity proportionally to the projected area of the suspended particles, and consequently proportional to the square of particle diameter. As the suspension settles, the projected area of the particles in the suspension decreases, and the intensity of the light beam increases.

The information obtained consists of the residual weight of suspended powder and, accordingly, the sediment accumulation after a given time, τ_x, allows us to calculate the particle size distribution on the base of the function $m = f(\tau)$ (see Figure 1.8) and Eqn 3. The particle sizes are presented here by their projected diameters (diameter of a circle equivalent to a particle projected area).

When X-rays are used to determine particle size distribution of a particle suspension, the attenuation of the X-ray beam intensity is proportional to the mass of the powder particles in contrast to their projected area in white light.

Method of weight samples

This method of particle size measurement, known as the pipette method, is based on Stokes's law. The pipette method consists of taking consecutive suspension samples of a certain volume from a given depth, h, at time, τ_i. The powder weight in suspension samples is determined after evaporation. Thus, in the pipette method, as in turbidimetry, the residual weight of the suspended powder at the fixed time is defined and, on the base of the function $R = f(\tau)$ and Eqn 3, the particle size distribution is calculated. However, in the pipette method, the residual weight of the suspended powder is defined directly in contrast to turbidimetry where an indirect method for its measurement is used. Figure 1.11 shows a schematic diagram of typical pipette devices. In practice, for the determination of particle size distribution, the Andreasen's pipette is still used.

Light Scattering

Light scattering measurements are based on the Mie theory [1]. Figure 1.12 represents schematically the principle of light laser scattering. Light scattering intensity obtained from Mie theory is described by the following equation:

$$K(\theta, m, D) = \frac{\lambda^2}{8\pi^2 R^2}[i(\theta, m) + i(\theta, m, D)] \quad (4)$$

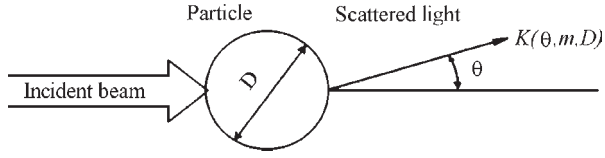

Figure 1.12 Laser scattering principle.

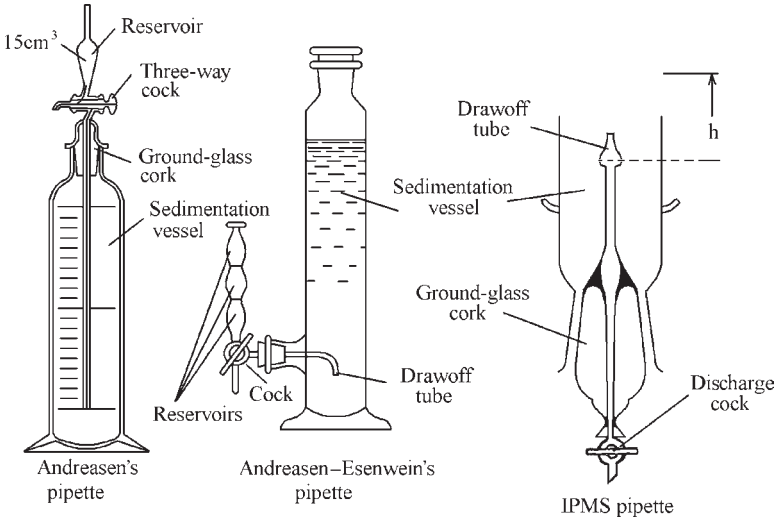

Figure 1.11 Pipette devices.

where $\pi D/\lambda$ is the size parameter, D is the particle diameter, λ is the incident light wavelength, R is the radial distance, $m = \mu_1/\mu_2$, μ_1 is the refractive index of the particle, μ_2 is the refractive index of the dispersing medium. The parameters λ and R are defined by the design of the instrument and are constant. Refractive indices (μ_1 and μ_2) in many cases are found in standard reference literature. In rare cases of newly developed materials or mixed dispersed systems, these values can be determined experimentally.

The complexity of exact solving of the Mie problem on the diffraction of electro-magnetic waves on a sphere or an ellipse generated numerous methods to simplify its solving, but the accuracy of particle size measurements is lowered. Modern computers make it possible to solve the complex Mie equation (4).

The light scattering method is capable of providing particle size analysis in a broad range of particle sizes. This technique ensures a rapid determination of the sought parameters, and is easy.

A typical recent device for laser light scattering measurement consists of a light source, particle dispersion and delivery systems, a detector to measure the light scattering by the specimen and a computer to control the system and to define the particle size distribution. Previous versions of laser particle analyzers were only capable of measuring the scattering pattern at small angles, lower than 20°, and were limited to measuring particles coarser than 1.0 μm. Modern instruments collect scattering data at larger angles. This allows accurate measuring of particles of 1.0 μm down to 0.1 μm in size. Particles in a parallel laser beam deflect the light at a fixed angle that depends on the particle diameter. A lens focuses the scattered light in a ring on the sensor that is mounted in the focal plane of the lens, whereas undiffracted light converges at the focal point on the optical axis. A certain scattering angle is allocated to each individual particle size. The energy distribution measured in the sensor elements that are arranged radially and symmetrically is evaluated, and the particle size distribution is calculated.

The major difficulty in accurate, reproducible particle size measuring is the dispersion. In previous instruments, the analyzer usually did not envisage this need. It was accepted that the dispersion would be performed external to the instrument particle analyzers. This, however, did not provide the stable dispersion and was not handy.

The recent instruments, such as for example, laser particle sizer 'Analysette 22' (produced by Fritsch company), are supplied with liquid and dry dispersing units. These two analyses give comparable results. For the liquid process, a mixture of liquids for suspension preparation is selected as for sedimentation analyses depending on the powder material composition (see Table 1.3). Usually, an integrated ultrasonic bath is used for the dispersion. The amount of sample required is approximately 0.2–1.0 g. The dispersing unit for dry samples processes the agglomerates by means of mechanical forces. A vibratory feeder meters the amount of sample supplied. Dispersion occurs in a two-phase annular gap nozzle due to cooling fins causing waves at the nozzle outlet with a high flow rate.

The popular tendency has been to incorporate a centrifugal pumping system. This type of pump provides sufficient power to pump particles of down to 2.0 mm in size around the system in a uniform condition. In this system, the ultrasonic probe is placed directly into the stream of the flowing liquid. The rapid flow rate and its position immediately in front of the cell where the laser beam is focused makes it possible to analyze even strongly agglomerating samples. These accessories have extended the range of samples that these instruments can analyze. Similar systems are incorporated into all newer devices.

There is also another tendency consisting of total removal of the pumping module from the system. This option is viable only for smaller particles; larger particles tend to become sediment below the laser beam. This approach is useful for analyzing particles in obnoxious fluids. It minimizes the use of the solvent and simplifies moving the sample.

The popularity in the last 10–15 years of laser light scattering as a method of particle size analysis has led to the development of new capabilities. The analysis has been automated and the reproducibility and the repeatability have been improved.

Surface and Bulk Characterization of Powders

Particle Image Analysis

Particle image analysis includes measurement of particle size, particle shape characterization, morphological analysis and surface chemistry analysis. Light microscopy is a very precise method of particle image analysis and allows us to observe and to measure individual particles. But some of the analyzing techniques used are more art than measurements. At the same time, the basic principles of sampling, preparation and measurement permit a precise count to be made with the thorough conception of the essence of the observable particles. Details of using optical microscopy for particle sizing are included

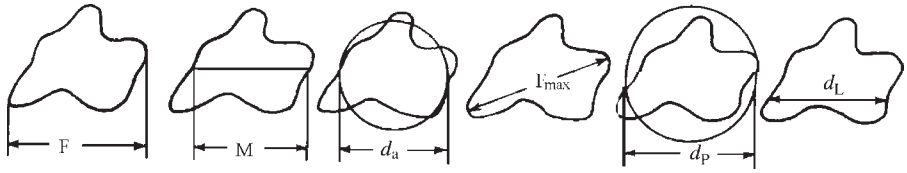

Figure 1.13 Measuring of irregular particles.

in ASTM standard E 20 and the Commonwealth of Independent States (CIS) standard GOST 25846 (see Appendix 1).

Size Measurements

These measurements consist of the determination of particle sizes, which are used to classify the two-dimensional particle images in terms of an equivalent spherical particle. Accepted particle measurements shown in Figure 1.13 include:

- d_F, the maximum length of the particle measured in a fixed position (called also Feret's diameter, *F*)
- d_M, the length of the line that bisects the area of the particle image, all particles being measured in the same direction (called Martin's diameter, *M*)
- d_a (project area diameter), the diameter of a circle with the same area as the two-dimensional image of the particle
- $d_{F\,max}$ (the longest diameter), maximum diameter of each particle, no set direction
- d_p (perimeter diameter), the diameter of a circle having the same circumference as the perimeter of the particle
- d_L (maximum horizontal intercept), the length of the longest line that can be drawn through the particle in a fixed direction.

The easiest for manual measuring is the diameter d_F. The average Feret's diameter, F_{av} is related to the perimeter of the convex hull of the particle P_{CH} and calculated by:

$$F_{av} = \frac{P_{CH}}{\pi}$$

Martin's diameter is related to the specific surface S_p of the particle by:

$$M = \frac{4}{S_p}$$

The first three diameters are related to one another by the expression $d_M < d_a < d_F$. The ratio d_F/d_M is used as a shape function, which is equal to 1.0 for spherical particles and increases in magnitude as particle shape becomes more irregular. The projected area diameter, d_a, gives the best evaluation of the accurate cross-sectional area of the particle.

The sampling techniques are described at the beginning of this chapter.

Particle Shape

Photomicrographs of several types of loose powders described in the International Standards Organization standard ISO 3252 (see Appendix 1) are shown in Figure I.2 in the Introduction to this book.

The British Standards Institute has prepared a standard glossary of terms for use in the description of the appearance of powder grains (British Standards 2955 Glossary of Terms Relating to Powders):

- *Acicular*: needle-shaped
- *Angular*: sharp-edged or roughly polyhedral shaped. (Polyhedral derives from poly, meaning many: therefore, polyhedral is understood to be a geometric shape having many faces, each of which can act as a base.)
- *Crystalline*: a geometric shape freely developed in liquid
- *Dendritic*: a branched crystalline shape
- *Fibrous*: regularly or irregularly threadlike
- *Flaky*: no normal definition in the British Standards. (It is assumed that a flaky fine particle is recognizable.)
- *Lamellar*: plate-like
- *Granular*: approximately equidimensional but irregularly shaped
- *Irregular*: lacking any symmetry
- *Modular*: rounded, irregularly shaped
- *Spherical*: globular shaped

Various shape terms have been proposed quantitatively to represent particle shape. Early systems tended to measure one specific feature of a particle.

There are known conventional shape factors [1], including the three ratios: elongation factor (x), bulkiness factor (y) and surface factor (z).

A rectangle of minimum area is drawn around the cross-section of a particle (particle projection). The ratio of the rectangle side length permits calculation of a particle's elongation factor:

$$x = \frac{a}{b}$$

where a and b are side lengths of rectangle.

The ratio of the area (A) of the projected particle to the area of the enveloping rectangle of minimum area ($a \times b$) indicates the bulkiness factor of the particle:

$$y = \frac{A}{a \times b}$$

Thus, the cross-sectional area of the particle is correlated with some of its linear dimensions.

To characterize the surface configuration by surface factor, which is an essential factor of shape, the surface of the respective particle should be compared with the surface of a sphere of equivalent volume or a cross-section should be compared with that of the particle:

$$z = \frac{c^2}{12.6A}$$

where c is the perimeter of the projection profile of the particles. For a spherical particle, $z = 1$, and for particles of other shape, $z > 1$.

Although the three ratios (x, y and z) do not permit exact characterization of particle shape, they are nevertheless descriptive.

Optical Microscopy

Optical microscopy allows the counting and sizing of particles from 100 to 0.5 µm in size. The depth of field of an optical microscope is about 10 µm at 100 and 0.5 µm at 1000 magnification. This requires the specimen powders to be placed in one plane and eliminates the wide particle size range by using automatic counting devices. Another limitation is that owing to the small number of particles usually counted, only the field of view can be characterized, not the representative lot from which the specimen was obtained.

Preparation techniques of slides for optical microscopy depend on the type of powder, particle size, particle size range and particle composition.

When a permanent slide is not required, and the powder develops good flow characteristics, slides can be prepared by applying dry powder onto the slide with a brush.

In conditions that require action to disperse the powder, a dispersing fluid can be used. The simplest technique involves placing a drop of the dispersing fluid on a glass slide and placing a small amount of powder onto the drop. This sample is then fixed by cover slip.

Obtaining permanent slides consists of preparation of thin films that can be produced by dissolving parlodion in amyl acetate, Canada balsam in xylene and polystyrene in xylene. Films are formed from a 0.5% solution directly on the glass slide. After the films dry, the powder is applied by spraying on the surface. The particles sink into the medium, forming a permanent slide.

A filar micrometer eyepiece is used for direct measuring of particle diameters in an optical microscope. This eyepiece contains a dial and a movable cross hair that is operated by a calibrated knob. During measuring, a particle is moved so that one side touches one of the fixed mesh markings, while the cross hair is moved to touch the other side of the particle. The difference between the two readings is the particle diameter, d_F, i.e. the maximum length of the particle measured in a fixed position, known also as the Feret's diameter [1]. This is a time-consuming technique. Eyepiece graticules are usually used to shorten the time required for particle size measurement.

A typical example of eyepiece graticules is given in British Standard 3406 (Figure 1.14) showing seven circles in a root-2 progression of sizes and five different geometric areas. A similar eyepiece graticule is used in the Commonwealth of Independent States. The last presents a disk comparator with ten circles and Vigdorchik's denumerably-measuring scale with twenty geometric areas [4].

These stencils are etched on glass disks that are positioned in the back focal plane of the microscope ocular and are thus in the same focal plane as the particle images. Feret's diameter, project area diameter (d_a), or perimeter diameter (d_p) (see Figure 1.13) are measured expediently with graticules.

Data Presentation

The percentage of fractions obtained as a result of analyzing the granulometric composition is conveniently presented in the form of a step-like graph (histogram). Particle sizes are plotted (at a uniform

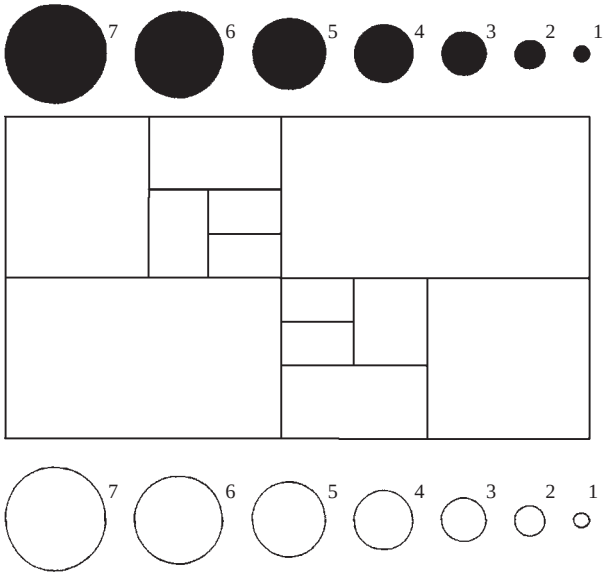

Figure 1.14 The British Standard eyepiece graticule for particle diameters measuring in optical microscope.

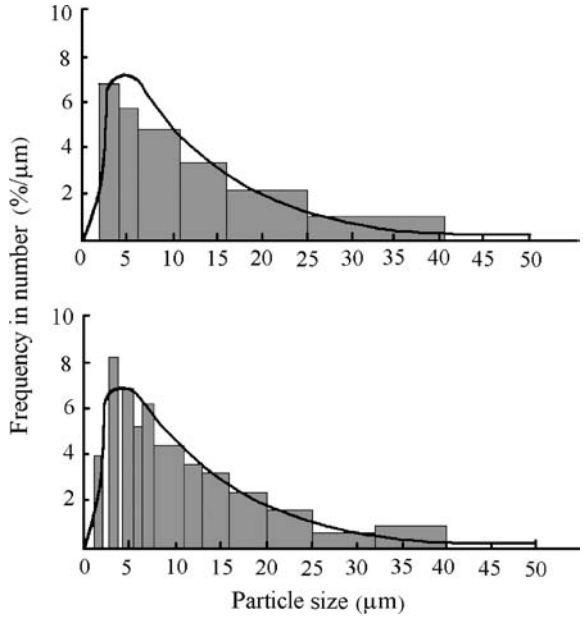

Figure 1.15 Histograms and size frequency curves of the two identical powder specimens by different particle size fraction ranges.

or non-uniform scale) as abscissas and relative fraction contents, i.e. percentages of each fraction, as ordinates.

In constructing the diagrams, it should be borne in mind that the ranges of separate fractions are usually taken to be non-equal. It is caused by technical conditions of analyzing as well as by the fact that, for a complete powder characteristic, the range of fractions should be increased with particle size increase. Indeed, the surface area of a particle of 1 μm in diameter is 4 times lower than the surface area of a particle of 2 μm in diameter, whereas for particles of 10 and 11 μm in diameter the difference in their surface areas is only 20%, and for particles of 100 and 101 μm in diameter it is as small as 2%. As powder properties significantly depend on their surface area, in the ranges coarser than 10 μm, a difference of 1–2 μm has a very small effect on particle properties and the separation into such small ranges is in this case non-expedient. Therefore, an increase of fraction ranges in geometric series with the growth of particle size seems to be justified.

In practice, the ranges of separate fractions are usually taken to be non-equal without a strict adherence to this condition. As a consequence, while constructing the histograms of weight distribution throughout particle sizes, the relative contents of fractions plotted on the ordinate are counted by dividing the weight percentage of each fraction by its range (difference in the limiting sizes in the fraction). The histogram gives a vivid presentation of powder disperse composition and the correctness of the presentation increases with narrowing the range limits. In Figure 1.15, the influence of the sizes of fraction range on the form of histograms is seen.

Metallographic Microscope

The requirement for the metallographic optical microscopes used for analyzing powders is that they form the image by a transmission principle. The powder sample is placed on a glass plate, each particle lying separately. Modern microscopes are equipped with digital photo-cameras and computers with a special program for powder analysis.

Techniques of Chemical Analysis for Powders

Chemical analysis of powders is carried out for quantitative and qualitative information. This is a complicated process with difficulties that can arise in the selection of the appropriate instrument and the correct interpretation of the results. The chart in Figure 1.16 can be used for the selection of the appropriate analytical technique.

Atomic absorption spectroscopy (AAS), atomic emission spectrometry (AES) and inductively coupled

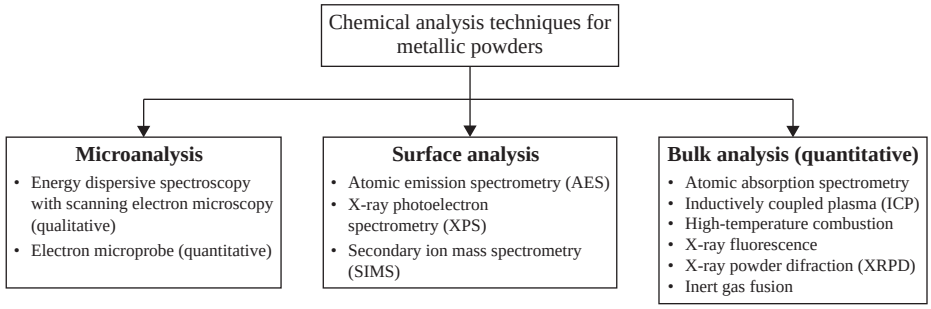

Figure 1.16 Chemical analysis techniques for metallic powders.

plasma optical emission spectroscopy (ICP-OES) are widely employed for chemical analysis of metal powders. AAS can detect the element content in parts per billion (ppb), but analyzes one element at a time. ICP-OES has a lower resolution, typically of 0.2–0.5 wt% for dissolved elements; however, the analysis ensures quantitative data for twenty or more elements simultaneously.

X-ray fluorescence allows the same broad element determination as ICP-OES; however, the material can be analyzed in the bulk solid condition. For trace analyses, this method has a lower resolution limit of approximately 100 ppm. The scanning electron microscopy (SEM) equipped with an energy dispersive spectroscopy (EDS) system can ensure a qualitative analysis of a metal particle. The microprobe analysis is regarded as microchemical analysis because of the small sample volume used to obtain the data.

Auger electron spectroscopy (AES), ion-scattering spectroscopy and X-ray photoelectron spectroscopy (XPS) can be used. The last is also known as electron spectroscopy for chemical analysis. Higher sensitivities are achievable by the use of the secondary ion mass spectrometry (SIMS). Microanalysis is also done with some SIMS techniques that can be used to measure composition and trace impurity levels as a function of depth, ensuring a detection limit in the ppb to ppm range for many elements.

X-ray diffraction analysis is one of the few methods that are available for a quantitative determination of the amount of phases existing in a powder sample. It should be remembered that the sensitivity of the X-ray diffraction technique in revealing the phase strongly depends on phase chemical composition and lattice type and is, in general, of about 3–5 vol%. X-ray diffractometers are widely used for this purpose, though the photographic technique can have a better sensitivity. The sensitivity can be strongly increased by using synchrotron radiation.

To obtain specific information for a particular phase in the powder (size and shape of phase particles, crystallographic orientation etc.) as well as to detect phases existing in a small amount, the transmission electron microscopy should be employed. Thin foils of about 0.2 μm in thickness are obtained from individual particles by microtome technique, most often with a fine diamond cutter [5]. In general, some defects are introduced into the foil in the cutting process, but for phase analysis it is quite suitable.

Scanning Electron Microscopy (SEM)

As a device for examining particle surfaces, the scanning electron microscope provides the following general possibilities: imaging of surface features is from 10 to 100 000×; resolution of features is from 3 to 100 nm depending on the sample; when equipped with a backscattered detector, this microscope allows us to observe grain boundaries on unetched surfaces; evaluation of the crystallographic orientations of grains down to 2–10 μm in size; and imaging of second phases on unetched surfaces when the second phase has a different average atomic number. This allows us to evaluate individual grains, precipitated phases and dendrites; to identify the chemistry of features down to micron sizes on the particle surface; to evaluate chemical composition gradients on the surface over distances approaching 1 μm.

Electron probe X-ray microanalysis provides qualitative and quantitative analysis of elements with atomic number of 11 (sodium) and greater with detection limits of approximately 1 μm, qualitative elemental analysis for light elements with atomic number from 5 (boron) to 10 (neon), and elemental compositional mapping of areas with dimensions as large as millimeters with spatial resolution to 1 μm. These capabilities are used for compositional analysis of individual phases at microstructural level in multiphase samples, analysis of compositional gradients close to boundaries, and compositional mapping of

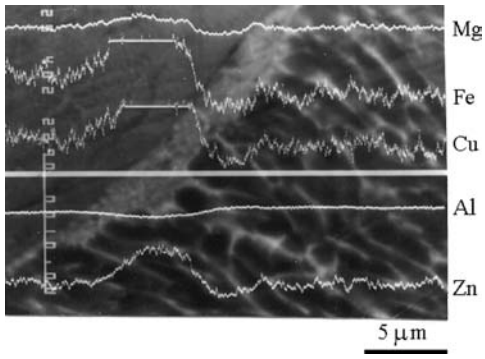

Figure 1.17 Scanning electron micrograph of the polished sample of Al-9.0Zn-3.0Mg-1.2Cu-1.0Fe alloy with elemental distribution along the secant line.

specimens to produce maps of element location and concentration.

Figure 1.17 illustrates an example of electron probe X-ray microanalysis for the analysis of element gradients at grain boundaries, in particle section along the secant line.

Auger Electron Spectroscopy

In Auger electron spectroscopy (AES), Auger electrons are produced whenever incident radiation (electrons, ions, photons or neutral atoms) interacts with an atom with an energy exceeding that necessary to remove an inner-shell electron (K, L, M,) from the atom. This scattering process leaves the atom in an excited state with a core hole, that is, a missing inner-shell electron.

In AES, the powder sample to be analyzed is bombarded with electrons. When an incident electron strikes a K-shell (core-level) electron with sufficient energy to free it, the atom is left in a singly ionized state with a core-level electron vacancy. If the atom is near the surface, both the incident electron and the core-level electron are emitted from the sample as backscattered electrons, with energies below approximately 25 eV.

These knockout results occur within to 3 nm depth under the surface that permits compositional analysis of the surface for all elements except hydrogen and helium. Auger analysis has some advantages for the analysis of light elements because the probability for Auger emission exceeds that for X-ray emission as atomic number decreases.

AES instrumentation typically includes an electron gun for primary electron excitation of the sample, an electron spectrometer for energy analysis of secondary electrons, a secondary electron detector for secondary electron imaging, a stage for sample manipulation and an ion gun for sputter removal of atoms from the sample surface. Depth-profiling analysis versus sputter is simultaneous or sequential.

Detection sensitivity for most elements (except hydrogen and helium) is from 0.1 to 1.0 at%. The accuracy of quantitative analysis is limited to ±30% of the element present when calculated using published elemental sensitivity factors. Better quantification (±10%) is possible by using standards that closely resemble the sample. Samples can be solid materials with relatively low vapor pressures at room temperature ($<10^{-8}$ torr). Higher vapor pressure materials can be handled by sample cooling or by applying a thin film onto a conductive substrate. Sample size can be individual powder particles as small as 1 μm in diameter. The maximum sample size depends on the specific device.

Secondary Ion Mass Spectrometry (SIMS) Analysis

The principle of SIMS consists of ion bombardment directed at the sample surface in a high or ultrahigh vacuum environment. The transfer of momentum from the impinging primary ions to the sample surface effects the sputtering of surface atoms and molecules. Some of the sputtering corpuscles are ejected with positive or negative charges that are termed secondary ions. These are then mass-analyzed using a double-focusing mass spectrometer or an energy filtered quadrupole mass spectrometer.

The method allows us to get a variety of information about the surface, subsurface or bulk composition of the sample. If the rate of sputtering is high, the intensity of peaks in the mass spectrum can be continuously recorded to provide an in-depth concentration profile of the near-surface region. At very high sputtering rates, trace element or impurity analysis in the bulk is possible.

Figure 1.18 illustrates an example of SIMS together with X-ray photoelectron spectroscopy (XPS) analysis of element depth distribution on particle surfaces. An O_2^+ primary beam was used to record positive secondary ions, while both O_2^+ and C^+ primary beams were used for analysis of negative secondary ions. The powder surface was scanned ranging from $35 \times 35\,\mu m^2$ to $50 \times 50\,\mu m^2$ with focused oxygen or cesium ion beams over an area. The spot size of the primary ion beam was approximately 3 μm. A mass resolution of $m/\Delta m = 300$ was used for all measurements.

Typical profiles of some elements are shown in Figure 1.18. Only Mg exhibits a pronounced enrichment of subsurface layers. Both Zn and Cu are distributed more or less homogeneously with some deviations from an ideal plane profile. Main metallic

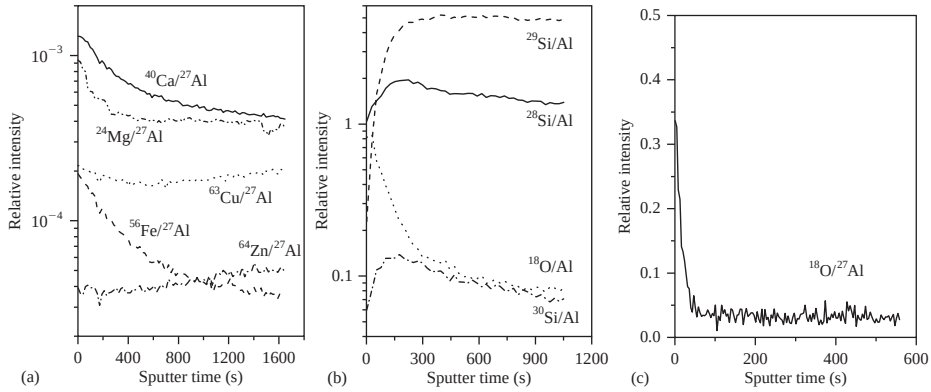

Figure 1.18 Typical depth profiles for: (a) Mg, Ca, Cu, Zn and Fe ions normalizsed to Al (primary O_2^+ and secondary positive ions); (b) Si and ^{18}O ions normalized to Al (primary Cs^+ and secondary negative ions); (c) $^{18}O/^{27}Al$ (primary O_2^+ and secondary negative ions).

impurities, Fe and Ca, are typically enriched in the subsurface as is seen from Figure 1.18a. The average thickness of the surface oxide film as well as the widths of the observed Mg, Fe and Ca segregation zones are estimated on the basis of the available depth profiles and respective ion sputter rate data. These thicknesses are taken to be proportional to the sputtering times required for a 50% drop in the element profiles [6, 7]. The average thickness of the surface oxide usually varies from 4 to 10 nm.The widths of Mg, Ca and Fe enrichment layers range between 30 and 70 nm.

Although a useful method of operation, it is not yet a routine analytical technique. More information on AES and SIMS methods can be found in http://www.cea.com/tutorial.htm.

Bulk Analysis

Many methods are available to determine the chemical composition of powders. A brief description of methods used in powder analysis is summarized below.

X-Ray Powder Diffraction (XRPD)

This technique allows us to make various investigations, including qualitative and quantitative phase identification and analysis, determination of crystallinity, lattice-parameters determinations, high-temperature studies, thin film characterization and analysis of crystal structure.

On the whole, an XRPD characterization of a substance consists of placing a powder sample in a collimated monochromatic X-ray beam. In XRPD analysis, samples are usually a fine powder fraction (ordinarily less than 50 μm in size). The particles in the sample comprise one or more independently diffracting regions that coherently diffract the X-ray beam. These small crystalline regions are termed crystallites. Although larger grain sizes can sometimes be used in XRPD, the size limitation is important because most applications of powder diffraction rely on X-ray signals from a statistical sample of crystallites. The angular position, θ, of the diffracted X-ray beam depends on the spacing, d, between planes of atoms in a crystalline phase and on the X-ray wavelength, λ, in accordance with the Wulf–Bragg equation:

$$2d \sin \theta = n\lambda$$

The intensity of the diffracted beam depends on the arrangement of the atoms on these planes. For the determination of the phase amount in the sample in the case of known phases, graphs constructed on the basis of X-ray patterns of standard mixtures can be used. A diffraction pattern can be recorded using film, analog or digital methods. Many modern automated powder diffractometers can provide further data reduction, including peak finding, a tabular listing of peak intensity versus interplanar spacing, and various computer utilities.

Phase identification using XRPD is based on the unique pattern produced by every crystalline phase. Qualitative identification of phases can be accomplished by pattern-recognition methods that include established manual techniques and the newer methods that use computers. All of these methods make use of the database maintained by the JCPDS International Centre for Diffraction Data (Joint Committee on Powder Diffraction Methods, International Centre for Diffraction Data, Swathmore, PA).

Inert Gas Fusion

This method is used to determine the quantitative content of oxygen, nitrogen and hydrogen in materials. Gases introduced into the material are quantitatively determined using inert gas fusion. Inert gas fusion reverses the physical and chemical bonding between the gases and metals to dissociate the gases and sweep them from the fusion area with an inert carrier gas. Because the gas/metal bonds are formed over a wide temperature range, bonds can be broken only by heating the sample above the highest temperature at which the gas/metal bonding occurred. Required powder sample mass is usually 2 g or less, depending on material type and the expected amount of gases present. Special precautions are required for metals with low boiling points. Materials with stabile nitrides or oxides require addition of fluxes. The method is destructive of the material.

Inductively Coupled Plasma Atomic Emission Spectroscopy (ICP-AES)

The ICP-AES is an analytical technique, based on the principles of atomic spectroscopy, for the determination of over 70 elements with detection limits in the parts per billion (ng/ml) to parts per million (μg/ml) range. In theory, the technique allows us to analyze all elements except argon. The samples can be introduced as liquids, solids or gases. In practice, favorable analytical results are obtained for approximately 70 elements, with detection limits usually reaching the ppb level, and most samples are introduced in liquid form as aqueous solutions. The inductive coupled plasma is the excitation source for atomic emission spectroscopy. Argon plasma operates at atmospheric pressure and is kept by inductive coupling to a radio frequency so that the standard frequency of operation is of 27.17 MHz or, less commonly, of 40.68 MHz (the frequencies permitted by the Federal Communication Commission for scientific and medical instrumentation [8]). The resulting plasma is a highly ionized gas with temperatures about 10 000 K. The ICP provides the capability of simultaneous multi-element analysis for as many as 60 elements in 1–2 min. The precision and accuracy are of the order of 1%.

Atomic Adsorption Spectrometry (AAS)

AAS is commonly used for the analysis of relatively low concentrations of approximately 70 metallic elements in solution samples [9].

There exist three types of AAS (Figure 1.19). Several features are common to all three techniques:

- flame atomic emission spectrometry (AES) (Figure 1.19a), where hot flame gases, to produce the desired signal, must thermally excite a significant fraction of the free atoms produced by dissociation in the atomizer from the ground-state level to one or more electronically excited states. AES usually necessitates scanning the monochromator completely over the analytical spectral line to obtain the background signal values necessary for the calculation of a correct response
- flame atomic absorption spectrometry (Figure 1.19b), where the radiation from a lamp emitting a discrete wavelength of light that has an energy corresponding to the difference in energies between the ground state and an excited state of the analyzed element is passed through the atomizer. Free analyzed atoms within the atomizer absorb source-lamp light at wavelengths within their absorption profiles. In contrast to AES, the ground-state (not excited state) atomic population is observed. The source light not absorbed in the atomizer passes through the monochromator to the light detector and the data reduction/display system of the spectrometer outputs an absorbance response directly proportional to the concentration of the analyzed atoms in the sample solution
- flame atomic fluorescence spectrometry (AFS) (Figure 1.19c) is an emission method based on an external light beam to excite analyte atoms radiatively. The absorption of light from the light source composes a higher count of excited-state atoms in the atomizer than that predicted by the Boltzmann equation at that temperature. Therefore, the absolute sizes of the atomic emission signals detected are larger than those seen in AES analysis performed with the same concentration of analyzed atoms within the atomizer. AFS has two major sources of error. The first is chemical scavenging of the non-equilibrium excited-state of the analyzed atom population before a useful light signal can be emitted. The second source of error is a scatter of the exacting radiation by particulate matter within the atomizer. For example, some refractory metals, such as zirconium and uranium, if present in high concentration in the sample, have a tendency to be incompletely dissociated or gasified in conventional atomizers.

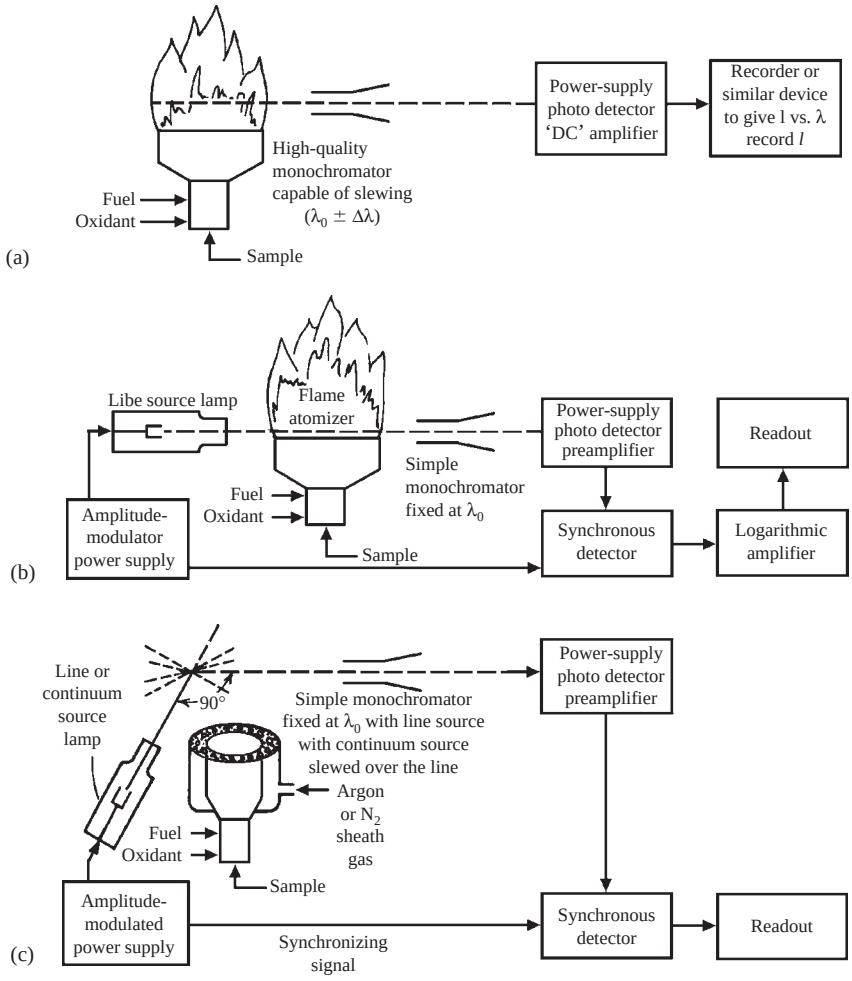

Figure 1.19 Comparison of (a) flame atomic emission spectrometry, (b) flame atomic absorption spectrometry, (c) flame atomic fluorescence spectrometry. (Source: Ref [9]®)

The sensitivity of atomic absorption spectroscopy is characterized by the magnitude of the atomic absorbance signal expected when a 1 ppm solution of the element is continuously aspirated into a flame atomizer or introduced as a discrete 25 µl aliquot into a graphite furnace.

On the whole, the AAS method has been one of the most widely used techniques of trace element analysis.

The capabilities of the contiguous techniques can be summarized as follows:

- Optical microscopy: provides superior image quality on relatively flat samples at less than 300 to 400×.
- X-ray diffraction: provides bulk crystallographic information.
- Scanning electron microscopy: minimum area for surface pictures of 4–5 nm (conventional scanning microscope), and for microchemical analysis of 1–3 µm (energy-dispersive spectrometry and/or wavelength-dispersive spectrometry).
- Scanning transmission electron microscopy: minimum area for surface pictures of 2–3 nm (SEM mode, in-lens), and for microchemical analysis of 5–30 nm (energy-dispersive spectrometry).
- Auger electron microscopy: minimum area for surface pictures of ≈100 nm (Auger), and of 10 nm (SEM mode), and for microchemical analysis of ≈100 nm (Auger), of 1–3 µm (energy-dispersive spectrometry).
- Transmission electron microscopy: provides information from within the volume of material, such as dislocation images, small angle boundary distribution, and vacancy clusters. The conventional resolution is of about 1–2 nm. A superior resolution requires very thin samples.

Determination of Oxygen Content by Reduction Methods

The methods for the determination of oxygen content by reduction in hydrogen are laid down in ISO 4491 Standard. They include: determination of loss of mass on hydrogen reduction (ISO 4491–2:1997), determination of reducible oxygen (ISO 4491–3:1997) and determination of total oxygen by reduction–extraction (ISO 4491–4:19889). Analogous standards function in the Commonwealth of Independent States (CIS): GOST 29006–91, GOST 27417–87 and GOST 18897–73 (see Appendix 1).

Standard ISO 4491–3:1997 establishes the technique for the determination of the oxygen content reduced by hydrogen in metallic powders that contain from 0.05 to 3 wt% of oxygen. This technique is applicable to powders of elemental metals and alloys. It cannot be used for powders containing a binder but can be extended over powders containing carbon by using a special catalytic device.

The principle of the process is in reducing a powder sample in the stream of pure dry hydrogen at a given temperature. The water formed by reduction is absorbed by methanol and titrated by Karl Fisher's reagent. In the case of analyzing powders containing carbon, a conversion of carbon monoxide and dioxide in methane with nickel catalyst is carried out.

The reduction is performed in an apparatus equipped with a reducing tube with closed end, or in an apparatus with a running reducing tube with open end (Figure 1.20). A weighed powder sample is from 1 to 5 g, depending on the oxygen content. The temperature and the optimum duration of the reduction are determined for each type of powder. Thus, the temperature for reducing oxides in nickel and cobalt powders is 900 ± 20°C with a duration of 20 min, and for molybdenum and tungsten oxides it is 1100 ± 20°C.

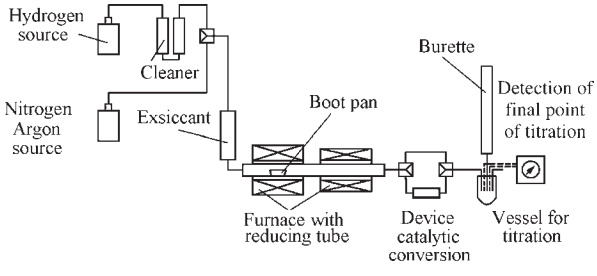

Figure 1.20 Flowchart of apparatus for oxygen content determination.

Surface Area and Porosity of Powders

The surface area in a quadratic degree, strongly depends on the powder particle size and not so strongly on their morphology and open porosity. At the same time, all these characteristics are significant factors for understanding and controlling product properties and processing behavior.

Various techniques can be used to determine these characteristics. However, the results of various test methods can differ owing to their inherent features. Mainly, the following methods to determine powder surface area, porosity and density are used: gas adsorption method, permeametry, pycnometry and mercury porosimetry.

Gas Adsorption

The gas adsorption technique is based on the Brunauer–Emmet–Teller (BET) model included in the determination of the amount of the gas that is adsorbed on the surface of the sample at low temperatures [10]. The specific surface area (m^2/g) defined by this method comprises the outward as well as the internal (open pores) surface area. However, the surface area of closed pores cannot be determined because of its inaccessibility for adsorbing gas molecules.

Brunauer, Emmett and Teller extended Langmuir's kinetic monolayer physical adsorption theory (1916) to a multilayer adsorption theory (1938). For convenience of a chart creation, the BET relationship is entered in the following form:

$$\frac{P}{V(P_0 - P)} = \frac{1}{V_m C} + \frac{C-1}{V_m C}\frac{P}{P_0} \tag{5}$$

The BET relationship is significantly complicated in the case when the number of adsorbed layers is limited:

$$\frac{V}{V_m} = \frac{C(P/P_0)}{1 - P/P_0}\,\frac{1-(n+1)(P/P_0)^n + n(P/P_0)^{n+1}}{1+(C-1)(P/P_0) - C(P/P_0)^{n+1}} \tag{6}$$

where V_m is the monolayer capacity; in the actual experiment, the adsorbed amount of gas, V, is measured as a function of gas pressure, P; P_0 is the saturation pressure of the liquefied gas at the corresponding temperature of the adsorption measurement; P/P_0 is often referred to as the relative pressure; the

parameters C and n are parts of the BET conception. The parameter C is:

$$C \approx \exp\left\{\frac{q_1 - q_c}{RT}\right\} \tag{7}$$

where the parameters q, R and T are the heat of adsorption, gas constant and temperature, respectively.

Due to the complexity of Eqn (6), it is seldom used in practice. Calculations are simplified by graphical construction. A diagram of $P/[V(P_0 - P)]$ dependence on P/P_0 in accordance with Eqn (5) generally gives a straight line in the range of $P/P_0 = 0.06$ to 0.3. The amount of gas adsorbed in a monomolecular layer, V_m, is determined from the slope of this line and its intercept with the ordinate axis. The total surface of the sample can then be calculated based on the specific size of the adsorbing molecule. It should also be taken into account that the value of C is rather sensitive to errors in the measurement and it can vary by 50% or more depending on how accurately the data points are taken and which data points are omitted in the calculation.

An isotherm of nitrogen adsorption on metallic powder surface of a typical gibbous shape of its initial part is illustrated in Figure 1.21. The initial supposition is that the process of the formation of the first adsorption layer on the surface of the powder sample is finished at point B of the beginning of the rectilinear section of the BC isotherm. A comparison of the values of monomolecular coatings

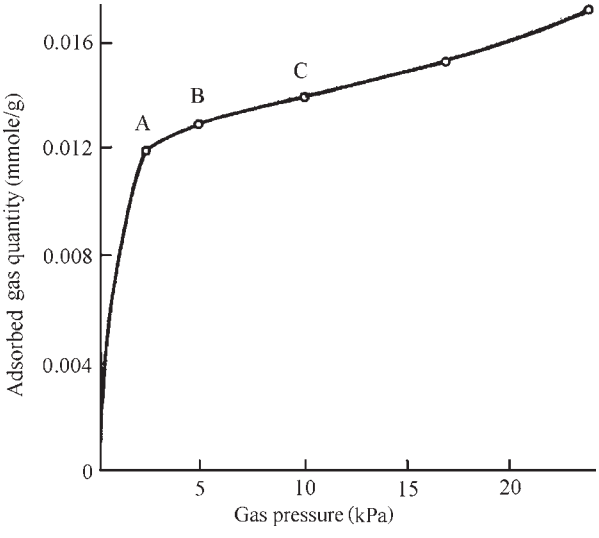

Figure 1.21 Adsorption nitrogen isotherm on metallic powder surface at 78 K.

by low temperature nitrogen adsorption (78 K) for different particulate materials calculated by the BET (V_m) technique and with the help of point B (V_b) in most cases show a satisfactory coincidence: the average value of the ratio V_b/V_m equals 0.97 and varies between 0.65 and 1.3 [11]. The results of investigations by the technique of low temperature (78 K) nitrogen adsorption of other authors for different metallic powders have shown the V_b/V_m ratio to lie between 0.9 and 1.04 [12].

In CIS countries, there is a standardized technique for the determination of the specific surface of metallic powders from 0.1 to 500 m^2/g by the thermal desorption of argon (Appendix 1, GOST 23401–90). The essence of the adsorption/desorption technique is in the determination of the amount of argon adsorbed on the surface of the adsorbent from the argon–helium mixture of a predetermined concentration at liquid nitrogen temperature and its subsequent desorption into the same mixture on increasing the temperature to 293 K. A maximum diversity between two parallel determinations does not exceed 20% for adsorbents with the specific surface from 0.1 to 10 m^2/g and 10% for adsorbents with the specific surface of 10 m^2/g and higher.

Gas adsorption/desorption methods can also be used to study the pore size distribution in the sample. Pores of up to 100 or 200 nm in size can be determined. The method is based on the capillary condensation, which means that a gas will condense into a liquid phase below its saturation point when it is confined in small pores. The fundamental relation between relative pressure and pore size is described by the Kelvin equation:

$$\ln\left(\frac{P}{P_0}\right) = -\left(\frac{2\gamma_{1v}V_1}{RTr}\right) \tag{8}$$

where γ_{1v} is the interfacial tension of the liquid–gas interface, V_1 is the molar volume of the liquid gas phase, and other symbols are gas constant, R, temperature, T, and radius of curvature of the liquid–gas interface, r. The adsorption/desorption isotherm shows a hysteresis and the relative pressure range where the hysteresis appears provides the information about the pore size. The explanation and the analysis of the hysteresis effect in more detail, including the information about network and connectivity effects of the pore system in a sample, are described in several manuals [13,14].

For the determination of the specific surface area various gases can be used. Usually, nitrogen or argon is used. The use of krypton or argon as the adsorbent improves the accuracy of measuring low specific surface areas.

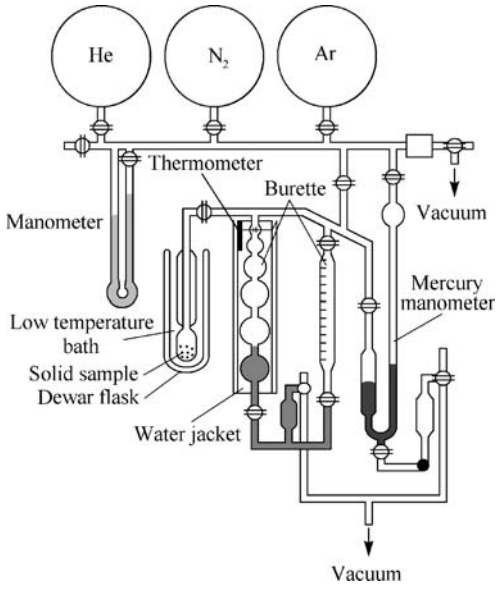

Figure 1.22 BET apparatus for specific surface area determination.

The apparatus for the determination of the specific surface area originally developed by Emmett is shown in Figure 1.22. Commercial instruments are now completely automated. In these devices, instead of the burette-type mechanism to measure the adsorbed gas volume, very precise pressure transducers are used to calculate the adsorbed amount from the known volume of a calibration chamber and the pressure drop that happens when the valve between sample and calibration chamber is opened. Further details are described in all manual books [13–15].

Permeametry

Among the indirect methods for the determination of powder specific surface, the methods based on measuring the gas permeability of the powder have gained ground. The quickness of the analysis and simplicity of the apparatus design have led to a wide usage of this method in industry.

Noteworthy is that, in all cases, the measured quantity is the resistance to fluid flow through a compact powder layer. In this way, the outer particle surface, as though 'smoothed out', without regard to their roughness and blind pores is determined, therefore the value of the permeability specific surface area (S_h) is even less than one determined by BET (S_{BET}).

The Kozeny–Carman equation is the widely used basis for all permeametry modifications. It expresses a connection between the pressure drop across the powder layer (ΔP), the velocity of fluid flow (ν) and parameters characterizing the powder layer including the permeable porosity (ε_v), the viscosity of fluid (η), the layer thickness (l), the average length of the path through the powder layer (l_0) and the density of powder material (ρ_p), and has the following form:

$$S_h^2 = \frac{l^2}{2\eta\nu l_0^2}\frac{\Delta p}{l}\frac{\varepsilon_v^2}{(1-\varepsilon_v)^3} \tag{9}$$

The method for the determination of specific surface of metallic powders by means of measuring the powder layer air-penetrability is laid down in ISO 10070. An analogous standard functions in the Commonwealth of Independent States (GOST 23401–90).

The value of the specific surface of powder, of which the permeable porosity is known, is determined by measuring volumetric flow (q) and the pressure drop of a dry gas (air as a rule) passing through the powder layer in laminar mode, and is calculated by equation:

$$S_h = \sqrt{\frac{\varepsilon_p^3 A\,\Delta p}{5.0(1-\varepsilon_p)^2 q\eta l\rho_p}} \tag{10}$$

where A is section area (m^2), ΔP(Pa), q(m^3/s), η(kg/(m · s)), l(m), ρ_p(kg/m^3) are as defined above.

The equivalent diameter of a spheroidal particle may be calculated as a diameter of the non-porous spheroidal particle having the same specific surface area as the particles of the investigated powder (measured by same method).

Commercial permeametry is applicable for powders with specific surface area and particle size in a range of 70–20,000 cm^2/g and of 0.5–50 μm, respectively [16, 17].

Several designs of permeametry apparatus are used. These instruments can be classified in two groups depending on whether the mass flow of the gas across the powder layer is constant or changing. The apparatus developed by Lea and Nurse [18] and Tovarov [4] (Figure 1.23) refer to the first group.

The Lea and Nurse apparatus was modified by Gooden and Smith by means of an addition of a self-calculating diagram that allows the direct readout of the specific surface. The commercial version of their modification is known as the Fisher subsieve sizer (Figure 1.24) [17].

The instruments of the second group are simplified in comparison with the first. The Blaine permeameter [15], IICX and ADII designs (Figure 1.25) [4] represent this type of apparatus. A variable pressure technique is used. Like this, a hand-operated pump in the form of a rubber pear is used in ADII apparatus.

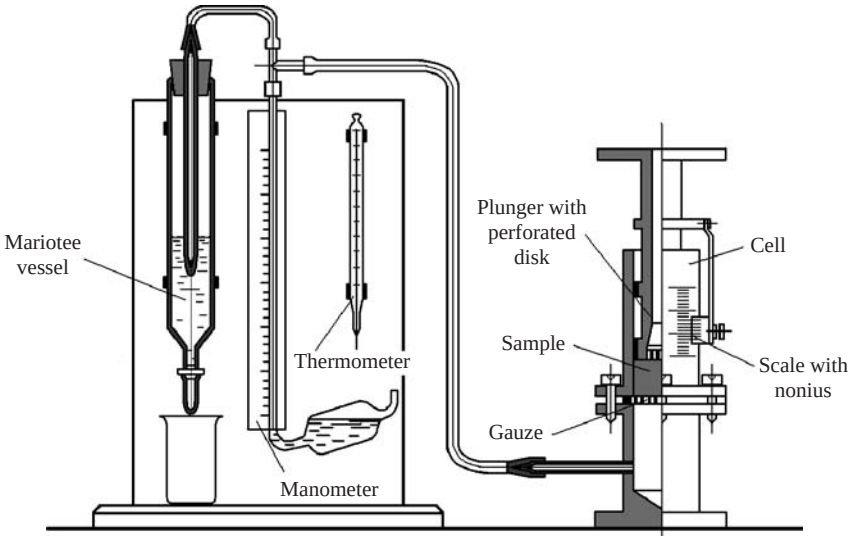

Figure 1.23 Tovarov's apparatus.

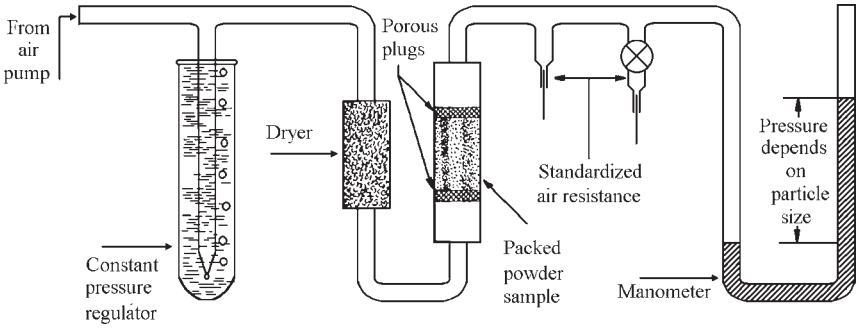

Figure 1.24 Fisher subsieve sizer.

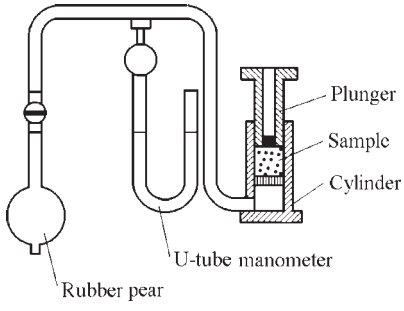

Figure 1.25 ADII apparatus for specific surface area determination.

A typical sample occupies a volume of about 5 cm^3 and, depending on its apparent density, is from 5 to 20 g in weight.

ADII apparatus consists of a cylinder (pan) with a perforated bottom, under which there is a connecting pipe for connecting the cylinder to the manometer. A hollow plunger is inserted into the cylinder, a circle of filter paper is put into the cylinder and a powder sample weighed to within ± 0.01 g is put in. The sample is coated with a circle of filter paper and is densified by a plunger. The height of the sample layer is measured by means of the points indicated on the plunger, then the plunger is removed and, by means of a rubber pear, the underpressure under the false bottom measured by the manometer is created. Underpressure gradually decreases due to air penetration through a layer. A stopwatch fixes the duration.

Using the empirical formula, powder specific surface (S, cm^2/g) is calculated:

$$s = k\frac{M\sqrt{t}}{P}$$

where K is the device constant (determined by a reference specimen); M is the coefficient found from the table for measured layer height and air temperature; t is the time of a manometric liquid lowering between two readings, s; P is the sample weight, g.

Specific surface determined by such a method characterizes the external surface of a powder without taking into account a relief of particle surface, their porosity, etc.

In the advanced design of the device, the evacuation with vibration at a frequency of 50 Hz is applied that prevents aggregation of particles and provides the stacking of particles with the porosity within the limits of 0.4–0.8. It increases the accuracy and reproducibility of the measurement.

Picnometry

Picnometry is used for the determination of the true density of PM materials. Density is one of the most important properties of metallic powders.

In addition to its use in measuring the true density of a powder, picnometry can also be used to discriminate among different crystalline phases or grades of materials, different alloys, compositions or prior treatments. Picnometry allows information to be obtained on the porosity of a material if the sample volume is known as well. Then the pore volume can be calculated as the difference between the bulk volume and specific volume.

Archimedes' law is the basis for defining the true density by means of the displacement principle. These can be measured using either liquid or gas picnometry. In liquid picnometry, the volume displacement is measured directly, as liquids are incompressible. The inability of the liquid to permeate pores, chemical reaction or adsorption onto the particle surface, wetting or interfacial tension problems lead to errors in density measurement. In these cases, the gas picnometry has an advantage over the liquid one.

Powder density defined by the liquid picnometry is calculated by the following expression:

$$\rho_p = \frac{m_2 - m}{V_p - V_L} \tag{11}$$

where m_2 is the weight of picnometer bottle with the powder and the liquid (g), m is the weight of the bottle with the liquid (g), V_L is the liquid volume in the picnometer (ml), V_p is the volume of the liquid with submerged powder in the bottle (ml).

In gas picnometry, the volume displacement is measured indirectly from the pressure/volume relationship of the gas under controlled conditions. Gas picnometry requires the use of high-purity, dry, inert, non-adsorbed gases such as argon, neon, dry nitrogen, dry air or helium. Of these, helium is recommended because it can penetrate into pores as small as 0.1 nm and behaves like an ideal gas.

In commercial picnometers, the powder sample is first conditioned to remove contaminants that fill or occlude pores and influence in such a way the surface characteristics. This is achieved by the exhaustion of the system and heating it to elevated temperatures followed by a purging with an inert gas. A typical commercial gas picnometer is a helium-filled sample system consisting of the sample cell, the calibrated reference cell, the vessel with a gas such as helium, the pressure transducer and the connecting pipes with flow control valves. This system is in 'zero' condition if it achieves the environmental pressure and temperature. At this point, the sample cell and the reference cell are isolated from each other and from the system by closed valves [19]. In the process of measuring, the gas is fed by opening the valves first into the reference cell, then it enters the sample cell where a given pressure value is established. Before the measurement in the sample cell starts, there is established a pressure P_2 that exceeds the ambient pressure by 100 kPa, then the pressure is elevated to the P_3 value.

The state of the system can be characterizsed by the equations:

$$PV = nRT \tag{12}$$

for the sample cell and

$$PV_R = n_R RT \tag{13}$$

for the calibrated reference cell and, when a solid sample of the volume V_S is placed in the sample cell

$$P(V - V_S) = n_1 RT \tag{14}$$

where P is the ambient pressure, Pa; V is the volume of the sealed empty sample cell, cm^3; V_R is the volume of the calibrated reference cell, cm^3; n is the amount of the gas (moles) in the sample cell volume at a pressure P; n_R is the amount of the gas (moles) in the reference cell volume at a pressure P; n_1 is the amount of the gas (moles) occupying the remaining volume in the sample cell at a pressure P; R is the universal gas constant; T is the ambient temperature, K.

Omitting the intermediate computations that characterize the changes of the gas state in the sample cell at a pressure of P_2 and the following pressure elevation, we deduce the expression for the gas volume V_S that penetrated into the pores at a pressure of P_3 (working equation):

$$V_s = V + V_R/[1 - (P_2/P_3)] \tag{15}$$

In recent years, the gas picnometer has been further improved by means of a more accurate pressure transducer, a better temperature control and automation. Modern picnometers can now reach an accuracy of 0.01% [19].

Porosimetry

Mercury and gas porosimetry are mutually complementing techniques with the former covering a much wider pore size range, from 0.3 mm to 3.5 nm, and the latter applicable to pores of 0.2 μm and smaller in size [20]. Mercury porosimetry consists of the step-by-step intrusion of mercury into an evacuated porous medium at increasing pressures followed by extrusion as the pressure is lowered.

Mercury porosimetry is based on the capillary rise phenomenon in which a surplus pressure is required to cause a non-wetting liquid to enter a narrow capillary. The pressure difference across the interface is described by the equation of Laplace (1806) and Young (1855), and its peculiarity is such that the pressure is lower if the contact angle θ (Figure 1.26) is greater than 90° or higher if θ is smaller than 90°. In the case of a capillary circular in cross-section and not too large in radius, the mercury meniscus will be approximately hemispherical. The curvature of the meniscus can be functionally related to the radius of the capillary that is given by Young–Laplace–Washburn equation (1921):

$$\Delta P = \frac{2\eta_{1v}}{r_p}\cos\theta \qquad (16)$$

where η_{1v} is the surface tension of the liquid (of 0.485 N/m for mercury), r_p is the capillary radius. The angle θ is the angle of contact between the liquid and the capillary walls.

Every mercury porosimeter contains a penetrometer unit into which the sample is placed. It is then evacuated to a given vacuum level before the sample cell is filled with mercury. The increasing pressure forces the mercury to penetrate into the largest pores in the sample. The amount of mercury penetrating into the sample is recorded at each pressure point respective to the pore size. The first reading is usually carried out at a pressure of 3 kPa, though a reading at a pressure of 0.07 kPa is possible [20]. The pressure is increased up to a final pressure of 400 MPa. Commercial units work either in a consecutive discrete or in a continuous mode. In the former, the pressure is increased in steps and the system is allowed to stabilize at each pressure point before the next step. In case of the continuous mode, the pressure is increased continuously at a given rate.

As is obvious (Eqn 16), two parameters play the most important role in the determination of pore size from the accurately measured applied pressure: the contact angle, θ, and the surface tension, $\eta_{1v.}$

The pressure is usually measured with an electronic pressure transducer or with a Heise–Bourden manometer used in older manual units.

Various methods are available to determine the contact angle.

Usually the sessile drop mode is used. A drop of mercury is placed on the flat surface of the sample and the resulting contact angle is observed visually and usually measured in its shadowgraph on a screen [21]. The same technique can be used to measure the contact angle in transparent capillaries. In the case of non-transparent capillaries, to obtain a shadowgraph such techniques as X-ray and ultrasonic flow-detection can be employed. It is necessary to take into account the difference between microscopic and macroscopic measurement of the contact angle under conditions of wetting and non-wetting [22].

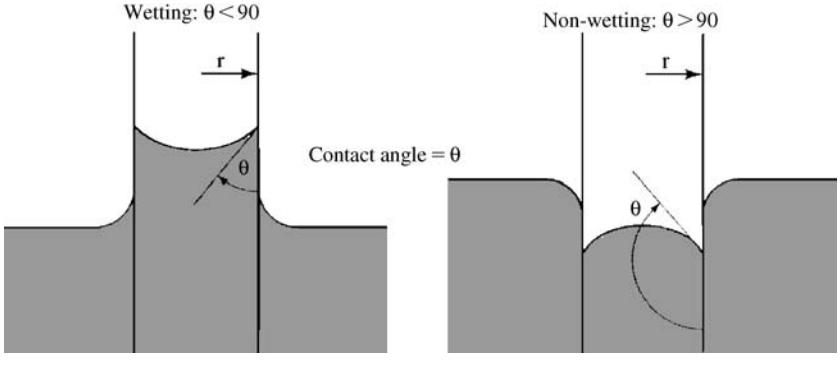

Figure 1.26 Contact angle (*θ*) of a liquid in capillary.

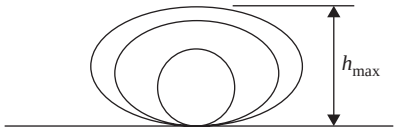

Figure 1.27 Change of mercury-drop shape with size.

Table 1.4 Contact angle between mercury and select PM non-ferrous materials

Powder	Angle (degrees)
Aluminum	140
Copper	116
Zinc	133
Tungsten carbide	121
Tungsten	135

The contact angle depends on the drop size (Figure 1.27). A simplified formula can be used when the maximum height of the drop, h_{max}, is determined:

$$\cos\theta = 1 - \frac{\rho g h_{max}^2}{2\eta_{lv}} \qquad (17)$$

where g is the acceleration of gravity and ρ is the density of the liquid.

The Willhelmy plate method [23] based on the effect of contact angle hysteresis for emersion and immersion is also known. Surface roughness or a change in surface composition during the contact with mercury can explain the presence of this difference. No surface roughness effects manifest themselves below pore size of about 100 nm.

Another technique consists in pressing a powder compact onto a disk with a well-defined hole. Mercury is now placed on the face plane of this disk and the contact angle can be calculated from the required pressure to force the mercury through this cylindrical pore with the size measured directly.

The contact angle, θ, is frequently supposed to be equal to 130° or 140°. This assumption is perhaps the largest source of error. The contact angles of mercury with various materials may significantly differ. Contact angle values between mercury and select PM non-ferrous metals [24] are shown in Table 1.4.

Samples of such metals as zinc, silver and lead can react with mercury. This can strongly change the non-wetting behavior of mercury with the sample. In this case, using a protective film, for example, of satiric acid formed on the pore surface can prevent this reaction. Moreover, for some reactive metals, such as aluminum, their natural oxide layer on the surface ensures sufficient protection.

Surface Tension of Mercury

The purity of mercury strongly influences the surface tension. Mercury is very sensitive to contamination and, probably for this reason, the evaluations of its surface tension values in earlier publications showed a lack of reproducibility. Later works [13], however, showed very consistent data. The effect of temperature is minimal, because the temperature coefficient of the surface tension of mercury is only of 2.1×10^{-4} N/(m°C).

Another error is caused by very small radii of pore surface curvature. The following correction has been suggested by Kloubek [25]:

$$\eta_{corr} = \eta - 2.66 \times 10^{-4}\ \Delta P$$

For $\Delta P = 200$ MPa, the correction term gives an error of 12%.

Restrictions and Limitations

The principal limitations of the results obtainable by mercury porosimetry are the following:

- The extent of the pore volume filled with mercury is limited by a maximum pressure. In such conditions mercury cannot penetrate into very small pores.
- Contrary to the former, the penetration into very large pores is limited by the height of the sample, which determines a minimum pressure. Consequently, very large pores may remain unfilled.
- In the process of porosity measurement, mercury not only penetrates into pores, but it also fills the space between particles that distorts the results obtained for the true volume of coarse pores.

Detailed discussion about restrictions and limitations of mercury porosimetry can be found in a series of works [26, 27].

Surface Area Determination

The surface area of a sample is calculated from mercury porosimetry measurements under a supposition of specific pore geometry. Many publications show a relatively good correlation between surface area values derived from mercury porosimetry measurements and corresponding nitrogen adsorption BET values (Table 1.5) [13, 24].

The value of the specific surface area is often used to calculate the contact angle of mercury on the

Table 1.5 Comparison of surface area measurements with nitrogen adsorption and mercury porosimetry

Sample	Surface area (m^2/g)	
	N_2-adsorption	Hg-porosimetry
Aluminum dust	1.14	1.35
Anatase powder	10.3	15.1
Boron nitride	20.0	19.6
Copper powder	0.49	0.34
Silver iodide	0.53	0.48
Tungsten powder	0.10	0.11
Zinc dust	0.32	0.34

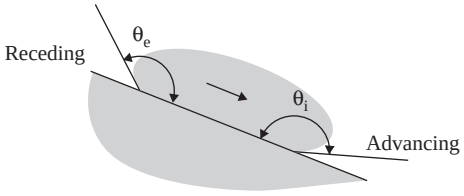

Figure 1.28 Contact advancing (θ_i) and receding (θ_e) angles.

sample material by varying the contact angle till the specific surface area computed from mercury porosimetry measurements correlates with the values determined from nitrogen adsorption data. This method might be a well-grounded alternative to determine the contact angle for materials that are able to withstand a strong effect of compressibility and have no pores smaller than about 10 nm.

Hysteresis and Detained Mercury

The interpretation of the penetration data from mercury porosimetry measurements has been mostly neglected because the interpretation was vague. Generally, three theories are used to explain the hysteresis between the intrusion and extrusion curves in mercury porosimetry measurements: contact angle hysteresis, ink-bottle theory, and connectivity model [27].

Numerous data of contact angle hysteresis indicate different values for advancing and receding contact angles (Figure 1.28). This model does not offer any explanation for the penetrated mercury that can remain in the sample pores after complete depressurization.

The ink-bottle model describes the condition in which mercury enters and leaves pores. It shows how some mercury remains trapped in the sample pores. However, for most samples, the ink-bottle theory prognosticates a much larger amount of mercury remaining in samples than one obtained in actual measurements.

The connectivity model represents a network of pores. In the regular network model, a porous medium is presented in the form of a regular two-dimensional or three-dimensional grid, the sites of which are connected by pores of a constant section. The main characteristics of the grid are obtained experimentally. The peculiarities of a real porous solid in its grid model are taken into account by the selection of the place of the principal pores volume concentration (in connections or in sites of the grid), the amount and the succession of the connections, the size of elements and their combination. This model probably describes the real condition better. However, in spite of a relatively large number of works in the field of mercury penetrability in porous media, the hysteresis problem remains unsolved to the present day.

Standardization

ASTM standards D 4284 [28] and C 493 [29] contain the recommendations for procedures accomplishing the mercury intrusion porometry.

Bubble Test of Pore Size

The essence of this method consists of measuring the pressure necessary for the appearance of the first air bubble on the surface of the sample completely saturated by a liquid to determine the maximum pore size, and in measuring a pressure that corresponds to the beginning of air bubbles discharge on the total sample surface to determine the average pore size. Ethyl alcohol is used as a liquid for sample saturation.

ISO 4003 standard establishes the recommendations for the procedures accomplishing the method of bubble test of pore size. An analogous standard is CIS (GOST 26849–86) (see Appendix 1).

Bulk Properties of Powders

Apparent density, tap density, angle of repose and flow rate are the main attributes that characterize bulk properties of powders. For accurate determination of these properties, a knowledge of the problems of powder movement plays an important part. Thus, the flow of metal powders in bins, hoppers, feeders, conveyors, as well as filling a die cavity is not always reliable or uniform. This often results in the press having to operate at pressing cycle times and wasted product due to composition or apparent density variations. A powder

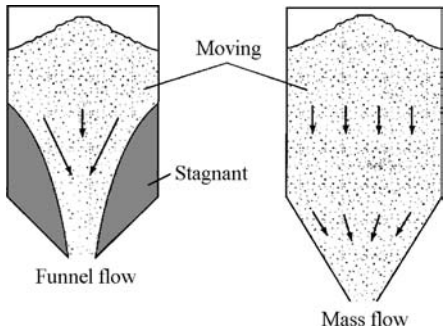

Figure 1.29 Two movement types of powder that can develop in the bin: funnel flow and mass flow.

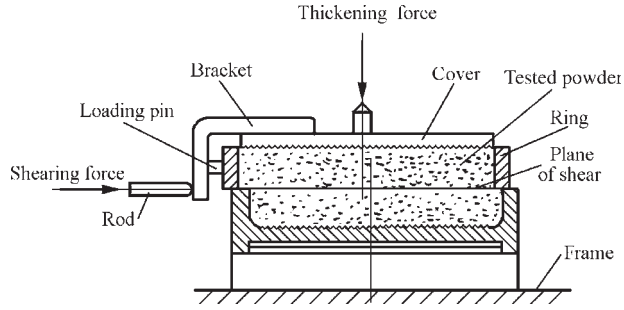

Figure 1.30 Jenike shear cell in initial offset shearing position.

may form a stable arch or a hollow; particle segregation may happen, that results in unacceptable variations in bulk density of the powder delivered to the feed shoe, or the powder may flood uncontrollably.

Bulk Flow Parameters

There are two virtual movement types that can develop in a bin: funnel flow and mass flow that are shown in Figure 1.29.

In funnel flow, an active flow channel is formed above the outlet with non-flowing powder at the periphery. As the level of powder in the bin decreases, layers of non-flowing powder may not slide into the flowing channel, which can result in the formation of stable hollows. Along with this, funnel flow can cause powder caking, form a first-in non-flowing powder, and increase the extent of sifting segregation.

In mass flow, all of the powder is in motion. Powder from the center as well as the periphery moves toward the outlet. Mass flow hoppers provide the flow sequence, eliminate stagnation of powder, reduce sifting segregation, and provide a steady discharge with a consistent bulk density and a flow that is continuous and well controlled. Conditions for the attainment of mass flow are accomplished by means of making the hopper walls smooth and steep as well as the outlet sufficiently large to prevent arching.

Having the information about bulk properties of powders, engineers can optimize the selection of storage and handling equipment. These same properties can be used to modify prevalent processes to correct flow problems. The following bulk solids handling properties are relevant to constitutive flow behavior: cohesive strength and frictional.

Cohesive Strength

When the powders are placed in bins, hoppers or containers, the consolidation pressures range from zero at the surface to relatively large values at increasing depth within the vessels. If a powder acquires a cohesive strength because of the pressures applied to it, an arch or hollow can form. An arch is a stable obstruction that forms over the point of narrowed cross-section of the vessel. The arch supports the rest of the contents vessel, hindering discharge. A hollow (called also a rathole) is a stable pipe or vertical cavity that connects with the outlet. Powder is left in stagnant zones that remain in their place until an external force is applied to destroy them.

The cohesive strength can be measured as a function of the applied consolidation pressure on a Jenike apparatus [30], shown in Figure 1.30 and accepted in ASTM D 6128 Standard [31]. The bottom of the cover and the inside of the base are roughened to increase friction with the powder under test. The base and the ring are filled with the powder being tested, and a vertical load is applied to the cover. A horizontal shearing force that acts on the section of contact between the ring and the base is transferred from the bracket to the ring through a loading pin. The standard shear cell is 95 mm in inside diameter. The present shear tester is equipped with a shear cell, a gravity vertical loading system and an electronic shearing force applicator with shearing rate of 2.54 mm/min. This arrangement produces a permanent record of the stress–strain relationship.

Shear testing is a two-step process that consists of consolidation (also called preshear) and shear. The consolidation is realized by accomplishment of specimen to flow under given stresses until a steady state is reached or closely approached. Measurement of the shear stress σ_{40} consists of obtaining its dependence on the pressure normal stress σ_p in yield locus. The determination of one yield locus requires the measurement of three to five points of the locus. For each point, the specimen is first consolidated and then sheared. The value of shear normal stress typically ranges between 25 and 80% of the preshear normal stress σ_p.

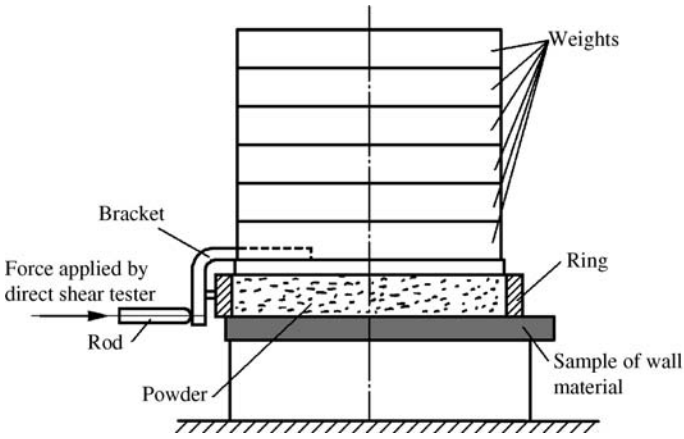

Figure 1.31 Shear cell used in measuring wall friction properties.

The flow condition of a powder is used for a variety of engineering decisions, for example, to design an optimal outlet assembly to prevent the formation of cohesive arches and ratholes. Details can be found in Jenike [30].

Moisture, particle size and shape, long-term storage at rest in vessels and some chemical additives influence the cohesiveness of the bulk powder.

Typically, cohesiveness rises as moisture content increases, but not in direct proportion. Hygroscopic materials can suffer significant increases during exposure to humid air.

As a rule, as a powder becomes finer, it also becomes more cohesive and difficult to handle. Dendritic, flaky or fiber particles are more cohesive than those that are spheroidal.

When a powder is kept in a bin or hopper for a period without moving, it can become more cohesive and difficult to handle. Such cohesion may result from settling and compaction, crystallization, adhesive bonding and agglomeration.

In some cases, adding a small amount of a chemical additive such as calcium, lithium or zinc stearate can make a cohesive powder flow more easily.

Frictional Properties

Both internal and external friction values can be determined by measuring cohesive strength with a shear tester (Figure 1.31) like the Jenike shear cell. Internal friction is conditioned by solid particles moving against each other and is characterized by the angle of internal friction and the effective angle of internal friction. External friction is characterized by the wall friction angle or coefficient of sliding friction. The higher the coefficient of sliding friction, the steeper the hopper walls that are necessary for mass powder flow.

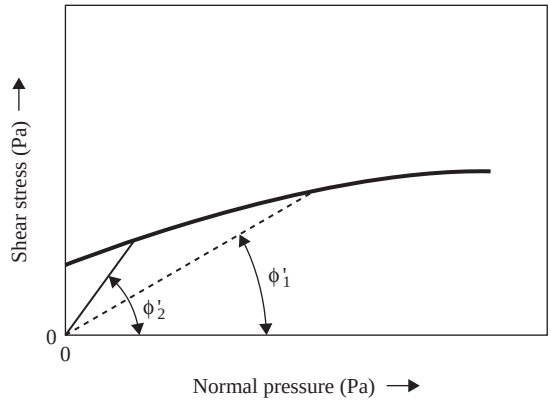

Figure 1.32 Typical results of the wall friction properties measured by means of shear cell test setup shown in Figure 1.31 to determine wall friction angle.

In the shear cell (Figure 1.31), a sample of wall material is placed on a disk so that the top surface of the wall material is the horizontal section of the force measuring stem. The ring is placed over the wall material sample and filled with the powder. After scraping off the excess powder, a cover is placed over the powder. A vertical force is applied to the cover by means of weight disks. This force creates a vertical pressure σ_w in the powder. Several (usually upto six) 0.5 or 1 kg weights are placed directly on the top of the cover of the shear cell to give the largest required normal pressure σ_w. The stem is moved. When the shear stress τ_w is leveled off with recording its value, one weight is removed. Thus, sequentially removing away the weights, the τ_w is determined for every magnitude of σ_w.

Characteristic results of the test for wall friction angle determination in the shear tester are shown in Figure 1.32. Typically, as vertical pressure increases, the wall friction angle decreases.

Table 1.6 Influence of particle size and particle shape on apparent density for several non-ferrous metal powders

Material	Manufacture method	Particle diameter (μm)	Specific surface Fisher (m^2/g)	Particle shape	Apparent density (g/cm^3)	Source
Aluminum	Granulation	500–2500	...	Needle	1.4	ECKA
Aluminum	Grinding	1000–2000	...	Irregular to semi-spheroidal	1.3	– " –
		500 max	...	– " –	0.8–1.2	– " –
		150 max	...	– " –	0.8–1.2	– " –
Aluminum	Air atomization	160 max	...	Irregular	1.0	– " –
		18 (a)	...	– " –	1.09	[32]
		15.5 (a)	...	– " –	0.98	– " –
		6.0 (b)	0.6	– " –	0.60	ECKA
Copper	Air atomization	500 max	...	Irregular	5.2	ECKA
		315 max	...	– " –	5.1	– " –
	Water atomization	315 max	...	Irregular	4.2	– " –
	Air atomization	160 max	...	Irregular	5.0	– " –
	Water atomization	100 max	...	Irregular	4.2	– " –
	Air atomization	63 max	...	Irregular	4.7	– " –
		45 max	...	– " –	4.4	– " –
	Grinding	...	0.3	Flake	1.1	– " –
		...	0.4	– " –	1.1	– " –
		...	1.0	– " –	0.8	– " –
	Electrodeposition	63 max	0.23	Dendritic	0.7	– " –
Zinc	Air atomization	315 max	...	Irregular	3.0	ECKA
		45 max	...	– " –		
Tin	Gas atomization	200 max	...	Teardrop-shaped	4.0	ESKA
		63 max	...	– " –	3.7	– " –
		40 max	...	– " –	3.5	– " –
		32 max	...	– " –	2.2	– " –
		8 (b)	0.25	– " –	2.0	– " –
Nickel	Carbonyl	3.2 (a)	...	Acicular	0.61	[32]
		3.8 (a)	...	– " –	1.87	– " –
		4.1 (a)	...	– " –	2.10	– " –
Nickel	Precipitation	3.5 (a)	...	Roundish	1.81	[32]
		4.4 (a)	...	– " –	2.09	– " –
		8.0 (a)	...	– " –	2.60	– " –

(a): Average particle diameter; (b): Median mass diameter; ESKA: ESKART- GRANULES Company

The pressure, moisture, particle size and shape, long-term of storage at rest in vessels, and wall surface condition influence both the internal and external friction values of metal powders.

Typically, as the consolidating pressure increases, the effective angle of friction decreases. Similarly, the coefficient of sliding friction often decreases as the pressure acting normal to the plate increases. When a powder is kept in a bin or a hopper for a period without moving, many powders experience an increase in friction between the particles and the wall surface.

Fine powders and those with a wide range of particle sizes are usually more frictional than coarse powders or those with a narrow particle size distribution. Dendritic, flaky or fiber particles are more frictional than roundish ones. An increase of moisture content in many powders leads to an increase in their friction.

The wall surface condition can appreciably manifest itself in sliding powders along it. Thus, smooth surfaces are typically less frictional.

Values of both internal friction angle and wall friction angle are required to design chutes, mass flow hoppers and other vessels.

Bulk Density

The term powder bulk density includes its apparent density and top density that differ from one another in their effect on compressibility of powder samples. This is one of the fundamental properties of a powder.

Apparent Density

Apparent density of metal powder is the weight of a unit volume of loose powder expressed in grams per cubic centimeter. This characteristic determines the actual volume allocated by a mass of loose powder that directly defines the processing parameters such as the design of consolidation tooling and the range of the press motions required to pack and to compact the loose powder.

Apparent density of a metal powder strongly depends on the particle size. Usually, it decreases with decreasing particle size. Table 1.6 shows the influence of particle size on the apparent density for several non-ferrous powders.

Apparent density decreases as the particle shape becomes more irregular, decreases with increasing surface roughness, and depends on particle size distribution. In the case of powders with a wide range of particle sizes, the apparent density increases because the space between coarse particles is filled with smaller particles.

Funnel Method

The most prevalent method for the determination of apparent density of metal powders uses the Hall funnel illustrated in Figure 1.33. ISO 3923/1 standard establishes recommendations for using this method with the application of the Hall funnel (Figure 1.33). An analogous standard functions in CIS (GOST 19440-94-86) (see Appendix 1). Both ASTM B 212 and MPIF Standard 04 describe this method of using the Hall funnel. Both ASTM B 417 and MPIF Standard 28 provide for the Carney funnel. This funnel differs in the design of the discharge opening (Figure 1.33). The orifice diameters amount to 2.5 and 5 mm, respectively.

The equipment assembly for the determination of the apparent density is shown in Figure 1.34.

Apparent density measurements are carried out by pouring powder into the funnel from which it flows into the 25 cm^3 density cup. After filling the cup, the funnel is moved away and the excess powder is leveled off using a spatula. The apparent density in grams per cubic centimeter is then defined by weighing the powder in the cup in grams and dividing by 25 cm^3.

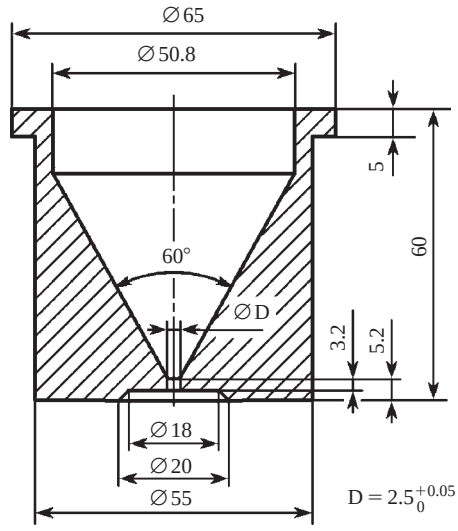

Figure 1.33 Hall funnel.

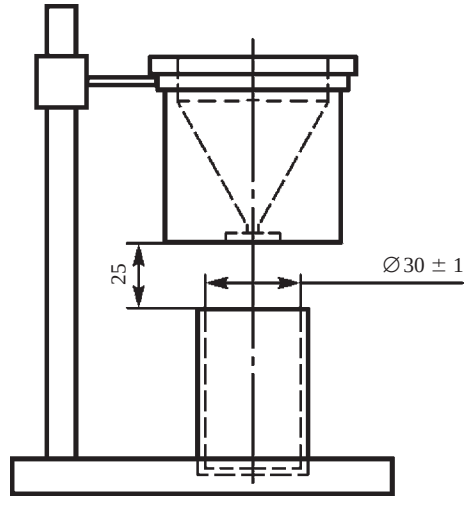

Figure 1.34 Equipment assembly for apparent density determination.

For powders that do not flow freely, the Carney funnel is used. The larger opening allows a greater variety of powders to flow. If the powder does not flow readily, its flow can be stimulated by poking a wire up and down in the orifice without entering the density cup.

Scott Volumeter

This method is used for powders that do not flow freely through a Carney funnel. In the Scott volumeter, the bulk condition of the powder is obtained

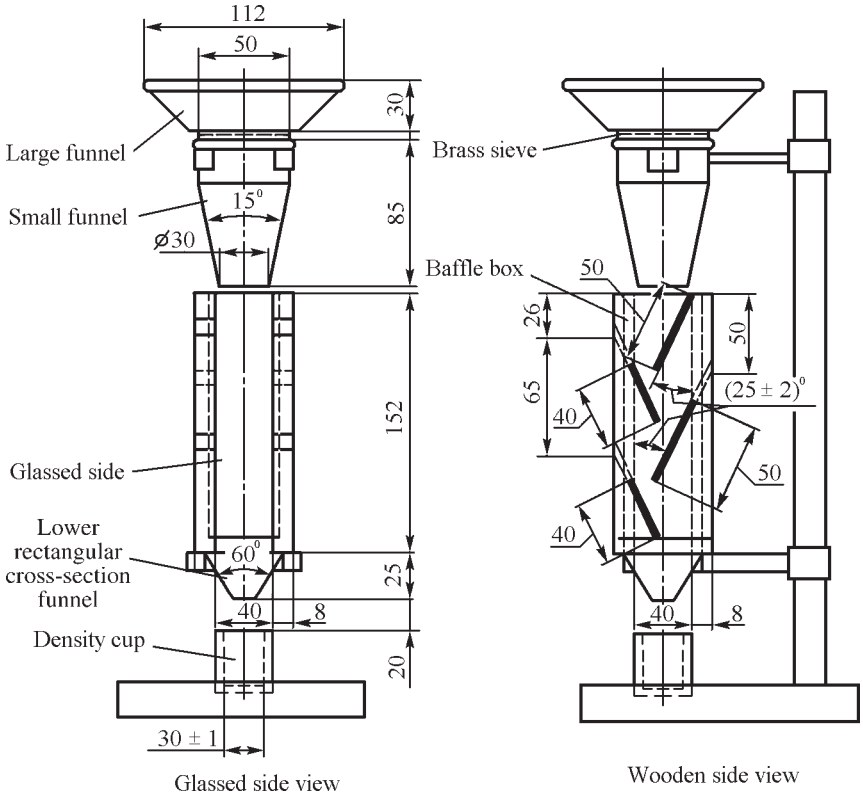

Figure 1.35 Scott volumeter.

by filling the density cup as a result of passing the gravitational powder jet through a system of inclined plates of the volumeter. As shown in Figure 1.35, the apparatus consists of a large funnel with a metallic screen and a smaller funnel that has a straight stem directing the powder into the baffle box. The latter with glass sides and two wooden sides contains a series of glass baffle plates and a funnel at the bottom to direct the powder into the density cup.

Pouring the test specimen carefully into the funnel begins the operating procedure. Ultrafine powders may require a light brushing with a synthetic brush to stimulate the powder to flow through the screen into the funnel. The powder is permitted to stream into the density cup until it completely fills and overflows the circumference of the cup. The excess powder should be removed from the cup by passing a spatula blade in flat contact with the top of the cup. The powder weight is determined accurate to 0.05 g. The density of the powder is given in grams per cubic centimeter if a metric cup is used, or grams per cubic inch if a non-metric cup is used.

Tap Density

The method for the determination of tap density, which is defined as the density of a powder when the volume container is tapped or vibrated under specified conditions, is established by ISO 3953. This method in accordance with ISO 3953 is accepted in ASTM B 527, MPIF 46, GOST 25279–93 and MIL-STD-1233 standards (see Appendix 1).

Tap density is a function of particle size distribution, particle shape and surface roughness. It is always higher than the free-flow apparent density.

A graduated glass cylinder with a volume of 100 ml and a multiplying factor of 0.2 ml (or a smaller graduated cylinder may be used for high-density powders) is used for tap density measurement. The amount of the powder for tap density testing is shown in Table 1.7. If mechanical tapping is used, the filled cylinder is placed in the mechanical apparatus, which operates till no further decrease in volume of the powder is observed (Figure 1.36). The amplitude of tapping or vibrating must be of 3 mm and frequency shall be from 100 to 300 impulses per minute. In both the latter or hand tapping, care must be taken to exclude loosening the surface layers of the sample during the procedure. The tap density in grams per cubic centimeter is then defined by weighing the powder in the cylinder in grams and dividing by the volume of the tapped powder in cubic centimeters. The results should be obtained with accuracy not worse than $\pm 0.1\ g/cm^3$.

Table 1.7 Typical tap density in comparison with apparent density of non-ferrous powders

Powder	Particle size (μm)	Apparent density (g/cm^3)	Particle size (μm)	Tap density (g/cm^3)	Increase (%)
Aluminum [32]	6.00 (a)	0.60 (b)	5.05 (a)	1.30	117
Cobalt [33]	99.6 wt% < 40 μm	1.8	99.6 wt% < 40 μm	3.0	67
Copper [34] (c): Spherical	...	4.5	...	5.3	18
Irregular	...	0.4	...	0.7	35
Flake	...	0.4	...	0.7	75
Nickel [35, 32]	3.0 (a)	1.0	3.0 (a)	1.9	90
Tin [32] (b):	8.0 (d)	2.0	2.45 (a)	3.15	57
Tungsten fine [36, 32]	3.27 (a)	2.16	1.15 (a)	4.45	106

(a): Fisher subsieve size; (b): ESKA Metal Powders; (c): Particle size distribution is the same for apparent and tap density; (d): Mass median particle size measured by means of laser granulometer

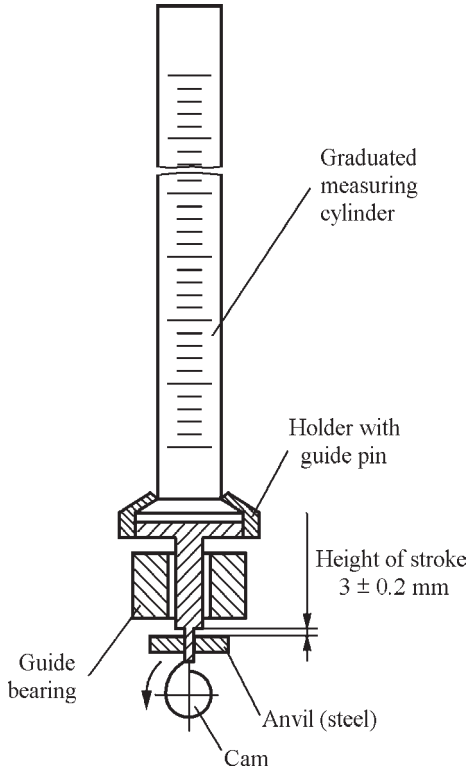

Figure 1.36 Diagram of tapping apparatus.

The amount of increase from apparent to tap density depends to a great extent on particle shape and particle size. Usually, the lower the apparent density, the higher the percentage increase in density on tapping.

Flow Rate

Flow rate is the time required for a powder sample of a standard weight (50 g) to flow gravitationally under atmospheric conditions through the Hall funnel into the cup. A determination of the flow rate of the powder is important in high-volume manufacturing, which depends on rapid, uniform, consistent filling of the die. Poor flow characteristics cause slow and non-uniform press feeding and even difficulty in filling of the die cavity. In modern automatic presses, the die cavity shall be filled with a certain constant amount of the powder in about 1 s.

ISO 4490 establishes the method of flow rate determination of metallic powders by means of the Hall funnel. The description of this method is contained also in ASTM B 213, MPIF 03 and GOST 20899-75 standards (see Appendix 1). Japanese standard JIS 7-2502-1966 and German standard 82–96 are standards equivalent to ISO 4490. The funnel with a calibrated orifice of 2.5 mm in diameter is made of aluminum alloy 6061–T6 with a smooth finish to minimize wall friction.

The test procedure consists of the following. A dry sample of 50 g in weight is poured into the funnel, the orifice of which is covered by the operator's finger. The stopwatch is started when the fingertip is removed and is stopped when the last powder leaves the funnel. The flow rate (s/50 g) of the sample is expressed as the time in seconds necessary for 50 g in weight of the powder to flow through the orifice. A powder that does not flow through the 2.5 mm orifice of a Hall funnel is classed as non-free-flowing powder.

The Hall funnel is calibrated using a standard powder (150-mesh Turkish corundum) that has a flow

rate of 40.0 s/50 g in the standard funnel. Real funnels can give somewhat different values of the flow rate of this powder due to peculiarities of their manufacture and this value is usually stamped on the funnel. The correction coefficient of the funnel equals 40.0 divided by this value. Calibration with Ballotini solid glass spheres with particle size ranges of 0.090 to 0.102 mm and 0.065 to 0.090 mm in diameters, has flow rates of 35.6 and 33.4 s/50 g, respectively.

Sliding at Impact Point

The chute angle and the roughness of the chute surface at the point of impact are the key factors in chute design. Optimum is the chute angle that does not facilitate an accelerated movement of powder in the chute with the transformation of constrained moving to free one, which is accompanied by a transition into suspension state of dust powder fractions (mainly of particles smaller than 50 μm in size) and by enhancing particle segregation in the reservoir filled with the powder. All of the factors affecting frictional properties can influence the optimum chute angle.

Segregation of Particles

A uniformity of the mixture is very important in achieving high-quality PM manufacture. In the case where a particulate material is represented by both a polydisperse powder and a mixture of powders differing in their physical–chemical properties, segregation results in the heterogeneity of the particle size distribution as well as of physical–chemical properties. This requires not only a proper mixing, but also suitable storing, feeding and transporting of powders.

Three phenomena have been identified as the primary cause of most segregation problems in metallic powders. They are the simple segregation mechanisms under gravity considered below.

Trajectory Effect

While pouring the powder by the chute onto the pile, particles are separated in size. The frictional drag on particles moving on a pile surface is higher for finer particles than for coarser particles. This results in a concentration of finer particles nearer to the end of the chute, while coarser particles come to rest at a much greater distance, to the base of the pile (Figure 1.37).

Screening Model (also called Sifting Phenomenon)

This effect occurs when finer particles move through a matrix of coarser particles. The screening effect occurs in typical PM processes connected with filling of different volumes. In these processes, there is revealed also an impingement effect when, under the impact of falling coarser particles, the pile of finer particles becomes more dense and that causes the slope angle of the upper part of the pile to become higher that the angle of repose (see Figure 1.37).

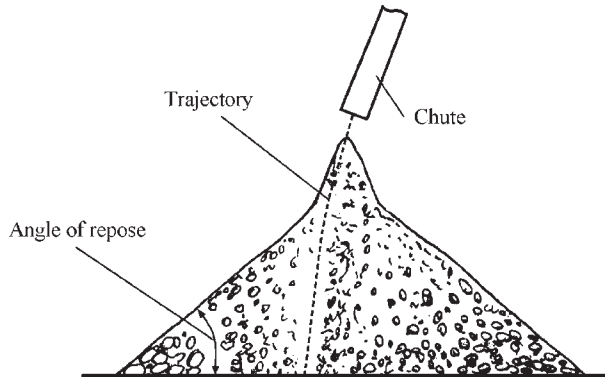

Figure 1.37 Trajectory effect segregation of particles.

Fluidization

Fine particles retain the ability to remain in suspension for a long time, whereas coarser particles settle first (according to their sedimentation rate). This results in a vertical segregation of particles within the powder layer. If the powder is segregated by air entrainment, fine particles will be located close to the top of the bottom-poured container. Air currents can carry the airborne fine and light particles away from a fill point to certain parts of a bin, such as toward vents and dust collectors.

Using the following data can help to influence the powder segregation during the production of PM parts:

- The more cohesive a powder, the less probable its segregation. Therefore, for some materials, the opportunity for segregation can be reduced by adding binders. This causes fine particles to stick to coarse ones and makes the powder less free-flowing. However, an additive must be optimized to avoid the possibility of reducing to zero the powder flow in the chute.
- The type of the displacement device can appreciably influence the segregation tendency of powders. It is significant that funnel flow patterns strengthen segregation, while a mass flow pattern tends to minimize such problems.

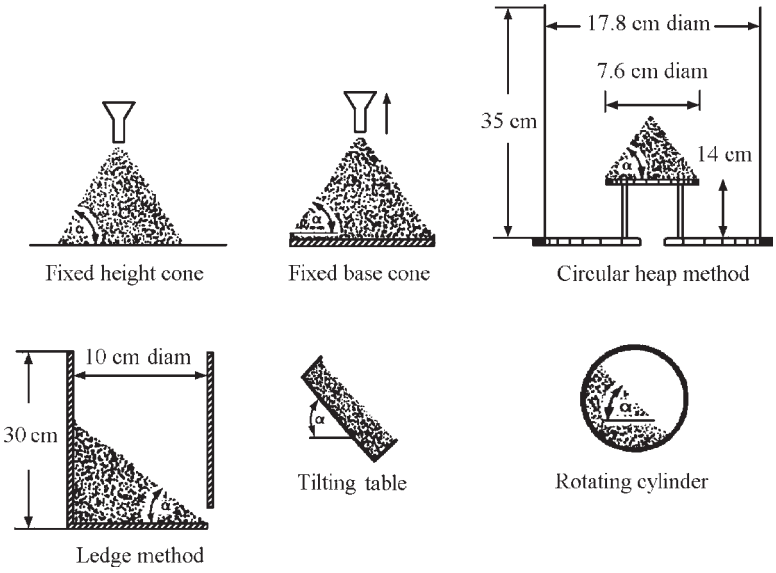

Figure 1.38 Six methods used to measure the angle of repose.

- Trajectory effect segregation is most likely to occur when the powder has a wide particle size distribution and when there is interparticle motion during operation. Usually, particles greater than about 100 μm in diameter are most subject to trajectory effect segregation. If most of the particles are smaller than 100 μm, the segregation by fluidization and particle entrainment is more probable.

Angle of Repose

The angle of repose is related to interparticle friction and the flowability of powders. It is not standardized. Several methods are used to measure this parameter. However, it is necessary to have in mind that the reliability of measuring the ultimate angle of repose depends on the measuring method used. Therefore, the measuring method should be carefully selected so that it best represents the property to be quantified.

A popular method for the determination of the angle of repose consists of the calculation of the tangent of the angle as the ratio of the height to the mean base radius of the powder heap. This powder cone is formed by means of carefully pouring the powder through a funnel. It can be formed as a fixed height cone, as a fixed base cone, or by means of using a circular method (Figure 1.38) measuring the angle.

The following methods have also found a use for measuring the angle of repose [37]:

- *Titling table*, where a rectangular box filled with powder is tilted until the contents begin to slide.

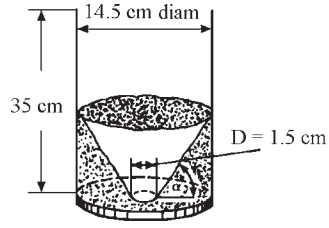

Figure 1.39 Crater method used to measure the angle of repose.

- *Rotating cylinder*, where a sealed hollow cylinder half full of powder is rotated until the powder surface shows its maximum angle with the horizontal. This angle is the angle of repose.
- *Ledge method*, where the powder is initially charged into a rectangular box (see Figure 1.38). A slot at the base of one vertical wall is closed by a board. The closure board is then removed to allow the material to flow slowly through the narrow slot. The angle with the horizontal plane of the surface of the powder equilibrium when the flow stops is calculated as the angle of repose.
- *Crater method* (called also *Discharge method* [38]), where a circular tube is placed vertically on a plate with an orifice in the center (Figure 1.39). The height of the remaining powder against the wall of the tube is measured at eight equidistant points around the circumference to determine the angle of repose [39].

- *Dynamic angle of repose* is determined in the apparatus consisting of a drum with a roughened internal surface that is half filled with powder and slowly rotated around its horizontal axis. Within a certain range of rotation speeds (usually from 2.5 to 6 rpm), the surface of the powder in the drum comes to a sufficiently steady condition. The maximum angle of bed inclination just before slump occurs is designated as the dynamic angle of repose [32].

Factors Influencing the Angle of Repose

There are internal and external factors affecting the angle of repose. Internal factors include particle size, particle shape and cohesiveness. Generally, coarser particles have higher angles of repose. However, very fine particles may reveal cohesiveness owing to the electrostatic effect, which increases the angle of repose. Typically, spherical particles have smaller angles of repose than irregularly shaped ones, owing to spherical particles having a greater tendency to roll.

External factors include the method of measurement and presence of other components including moisture. The effect of measuring method is discussed in detail above. It is significant that the ledge and crater methods give a higher angle of repose than that obtained from the heap formation methods. The angle of repose of loose dry powder increases by compacting, as well as by introducing moisture.

Compactibility of Metal Powders

Compressibility and compactibility define the ability to form unsintered ('green') compacts by die pressing of powders. Generally, the compressibility is quantified as the value of the compacting pressure required to ensure a specified green density of the sample. Therefore, the compressibility of the powder is an important factor in the design of pressing equipment. It is usually expressed in terms of green density. The compressibility is also measured by the compression ratio, which is the ratio of the green density to the apparent density of the powder.

The compactibility is evaluated by the green strength of a powder compact and relates to the sample complexity, fragility and the ability of the compact to be ejected from the die. The relation between the compressibility and the compactibility is complex, because some factors can improve one of them to the detriment of the other. Thus, particles of a spherical shape generally have a higher compressibility. In contrast, an increase of particle surface area, which can be achieved by increasing the particle surface irregularity, usually increases the green strength. At the same time, such factors as increasing the compaction pressure and the temperature have competing effects on the compressibility and the green strength. These factors promote intense particle movement and deformation, which are the bases to improve mechanical interlocking.

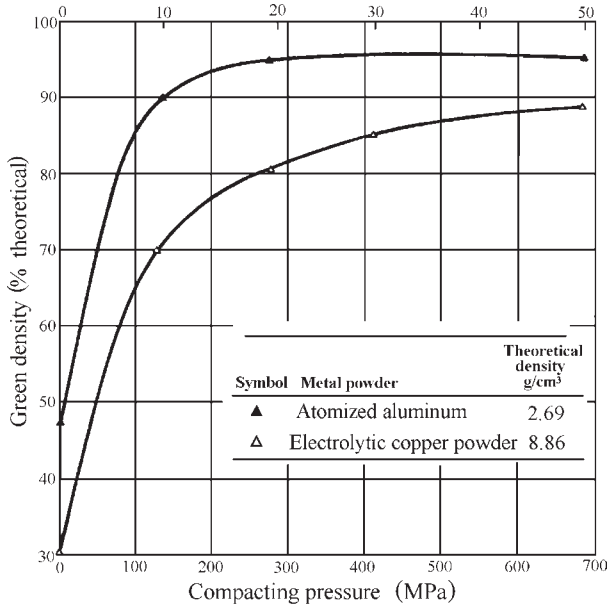

Figure 1.40 Compressibility curves for gas atomized aluminum powder and electrolytic copper powder.

Compressibility

Characteristic compressibility data for gas atomized aluminum powder and electrolytic copper powder are shown in Figure 1.40 as a functional dependence of the percentage of the theoretical density on the compacting pressure [40].

Lubricants are used to promote the ejection of the compacted samples from the die. At higher compacting pressures, lubricants reduce the green density owing to the fact that they are taken up by the available pores. There are two lubrication techniques. One method consists of mixing a dry lubricant such as zinc stearate, amide wax and stearic acid, with the metallic powder. By the other method, the die walls and punches are greased by the lubricants. In the case of the powder lubrication method, the lubricant addition may range from 0.5 to 1.5 wt%. With the wall lubrication, a solid lubricant is mixed with a volatile organic liquid, for example 100 g zinc

stearate with 1 l methylchloroform. This mix is either painted or sprayed on the tooling. The organic liquid evaporates, leaving a thin film of dry lubricant on the working surface of the die cavity and punches.

ISO 3927, 'Metallic Powders Excluding Powders for Hardmetals – Determination of Compactibility (Compressibility) in Uniaxial Compression', establishes the method for the compressibility. The description of this method is contained also in ASTM B331, MPIF 45 and GOST 25290-90 standards (see Appendix 1).

For pressing, dies of tool steel hard metal are used, one of them for cylindrical and the other for rectangular compacts. The cylindrical die shall ensure the manufacture of compacts of 20–26 mm in diameter and with the height-to-diameter ratio of 0.8–1.0, and the rectangular die shall ensure the manufacture of compacts in the form of plates of $30 \times 12\,\text{mm}^2$ in size and of 5–7 mm in thickness. The shaping is carried out in a press with the loading to 500 kN, which is controlled for a uniform growth with a rate not higher than of 50 kN/s. To construct the curve of powder compressibility at repeated pressing, loadings of 200, 400, 500, 600 and 800 MPa are used. If the compressibility at a single pressing is needed, it is measured at one of the above pressure values.

After pressing, the green samples are weighed to ± 1 mg and their sizes are measured by a micrometer to ± 1 μm. The compressibility (ρ_p) that is determined by the density of the pressed sample is calculated by the formula:

$$\rho_p = \frac{m}{V}$$

where ρ_p is the compressibility, g/cm^3; m is the weight of the green compact, g; V is the volume of the green compact, cm^3.

Green Strength

Necessary and sufficient mechanical strength of a cold pressed green specimen allows the ejection of the green specimen from the die and its transfer to the sintering furnace or die head without breakage. This is particularly important for thin-walled specimens, thin sections of large parts and finned specimens. The strength of green compacts depends mainly on mechanical interpenetration of superficial irregularities of particles, which is favored by plastic deformation during pressing. Therefore, spherical particles show the lowest degree of mechanical strength because of low initial surface contact between neighboring particles. Green strength is also decreased when oxidation and contamination of particle surfaces and the amount of adsorbed gases increase.

Standard test methods to determine green strength of an unsintered compact are specified in ISO 3995, 'Metallic Powders – Determination of Green Strength by Transverse Rupture of Rectangular Compacts'; the description of this method is contained also in ASTM B312, MPIF 15 and GOST 25282-93 standards (see Appendix 1).

The main point of the method consists of the determination of the bending stress of green samples of a rectangular section by means of the action on the sample of a uniformly growing load up to fracture. The strength is determined as the stress calculated by the bending equation that is necessary to crack the rectangular billet installed on the two supports along the edges and subjected to the load imposed in the centre. An example of the device for testing the sample strength is shown in Figure 1.41.

For the test, samples of not less that 30 mm in length, 10–13 mm in width and 5.5–6.5 mm in thickness are used. The load is increased with a constant rate till the sample fails (not quicker than 10 s). The strength of the non-sintered material is calculated by the formula:

$$S = \frac{3PL}{2t^2W}$$

where S is the green strength, MPa; P is the force at the instant of the failure, N; L is the distance between the supports, mm; t is the thickness of the specimen, mm; W is the width of the specimen cross section, mm.

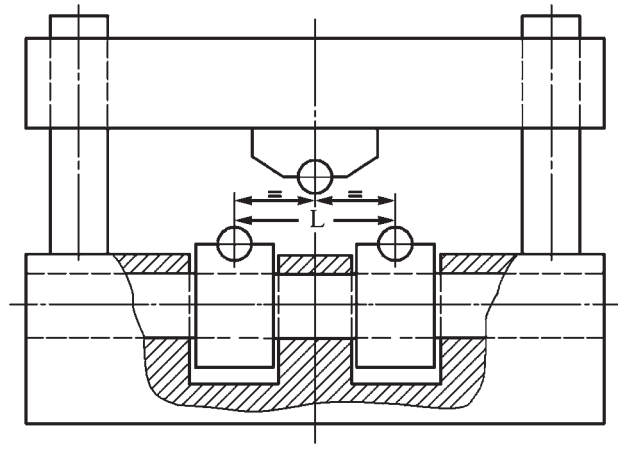

Figure 1.41 Device for testing of green strength of an unsintered compact.

Table 1.8 Apparatus for powder analysis

Apparatus	Principle of operation	Measurement range (μm)	Measuring time	Source
Particle size analysis techniques				
SediGraph III 5120 particle size analyzer	It determines particle size by using the sedimentation technique which measures, with the help of narrow X-ray beam, the settling rates of different size particles in a liquid with known properties	Particles ranging from 300 to 0.10 μm equivalent spherical diameter	Runs up to 18 samples unattended operation in 15 minutes max	MIC
Saturn DigiSizer	The digital presentation of the pattern is obtained as a result of laser light scattering from a sample. The resulting information is then processed using data reduction based on Mie theory	Particles ranging from 1000 to 0.10 μm equivalent spherical diameter. Accuracy in particle range: from 0.10 to 1.0 μm relative error amounts 10%; from 1.0 to 1000 μm one 3%	Approx. 10 s	MIC
Laser-Particle-Sizer 'analysette 22' (comfort)	Method utilizes a principle of the scattering of electromagnetic waves to determine particle size distribution	• Liquid dispersing unit: from 0.1 to 1250 μm • Dry dispersing unit: from 0.8 to 1250 μm • Free-flowing samples: from 0.8 to 1250 μm	Approx. 10 s	Fr
Surface area, porosity and density measurements				
TriStar 3000	Surface area determination and porosimetry are based on the technique of gas adsorption	Measures surface are as low as 0.01 m^2/g	Performs three BET surface area measurements in approx. 20 minutes	MIC
ASAP 2020	Surface area and porosimetry analyzer uses the gas sorption technique to determine the percent metal dispersion, active metal surface area, size of particles, and surface acidity of catalyst materials	Pressure range: 0 to 950 mmHg	Accuracy: • 1000 mmHg range: within 0.15% of reading (high vacuum systems); • 1 mmHg range: within 0.12% of reading (micropore)	MIC
FlowSorb III	It measures surface area using the flowing gas method, which involves the continuous flow of the adsorptive and inert gas mixture over the sample at atmospheric pressure	Samples with surface areas from 0.01 m^2/g to 1000 m^2/g	Reproducibility is better than 0.5%	MIC
AutoPore IV 9500	Porosity of material is characterized by applying various levels of pressure to a sample immersed in mercury	Ability to measure pore diameters from 0.003 to 360 μm	Better than 0.1 μl for mercury intrusion and extrusion volumes	MIC
MultiVolume Pycnometer 1305	Method utilizes a principle of gas picnometry, where volume displacement is determined from the pressure/volume relationship of a gas, preferably helium, under controlled conditions	Range of sample volumes: from 0.5 to 150 cm^3	Accuracy: of ±0.1 to 0.2%	MIC

MIC: Micromeritics Instrument Corporation. More information on these apparatuses can be found in http: www.micromeritics.com; Fr: Fritsch GmbH (Germany)

For most applications, green strength values of 5.0–6.0 MPa or higher allow safe handling of green specimens. Lower green strength may cause horizontal lamination in the specimen. Specimens with sharp contours or thin sections, or specimens made from a blend of several powders in which some of the components detract from the overall strength of the specimen, require higher green strength characteristics.

Apparatus for Powder Analysis

Several advanced designs of apparatus for powder analysis have been developed in recent years. These include the particle size techniques as well as surface area, porosity and density measurements. Table 1.8 contains the list of some of these devices.

Laser particle sizer 'analysette 22' Comfort from Fritsch GmbH (Germany) is a versatile instrument for determination of the size distribution of suspensions, emulsions and powders. The usable inverse Fourier optics provides measurement of particle size distribution with a very high resolution. With the computer-controlled location of the measuring cell (max. 310 positions) in the convergent beam between laser and sensor, it is possible to utilize up to 310 measurement signals for the calculation. The new generation SediGraph III 5120 Particle Size Analyz with advanced instrumentation from Micromeritics Instrument Corporation (United States/Germany/Italy) provides accurate and reproducible results. Particles with diameters in the range of 300 to 0.1 μm can be measured. Scanning the sedimentation cell from bottom to top permits accurate inventory of particles while minimizing the time required to resolve the separation of fine particles. Vibratory sieve 'analysette 3 M' from Fritsch GmbH provides microprecision sieving with automatic weighing of sieve sets, while particle size distribution is determined by sieving. The TriStar 3000 gas adsorption analyzer from Micromeritics Instrument Corporation is a fully automated surface area and porosimetry analyzer, providing three BET surface area measurements simultaneously in approximately 20 minutes. The AutoPore IV 9500 Series from Micromeritics Instrument Corporation characterizes a material's porosity by applying various levels of pressure to a sample immersed in mercury. Mercury porosimetry is applied over a capillary diameter range from 0.003 to 360 μm. The operating details and special features of these devices can be found in the respective brochures available from the manufacturers.

References

1. Allen, T., *Particle Size Measurements*, 4th edn. Chapman & Hall Publishers, 1990.
2. Allen, T., Sampling and classification of powders. In *ASM Handbook*, Vol. 7. ASM International Publishers, 1998, pp. 205–221.
3. Pope, L.R., Ward, Ch.W., *Manual on Test Sieving Methods*, 4th edn. ASTM Publisher, Mayfield, PA, 1998.
4. Kouzov, P.A., *Fundamentals of Particle-Size Analysis of Industrial Dusts and Particulate Materials*. Himiy Publishers, Leningrad, 1987 (in Russian).
5. Shimizu, K., Brown, G.M., Kobayashi, K., Skeldon, P., Thompson, G.E., Wood, G.C., Ultramicrotomy – a route towards the enhanced understanding of the corrosion and filming behaviour of aluminium and its alloys. *Corrosion Science*, 1988, 40(7):1049–1072.
6. Krajnikov, A., Gastel, M., Orter, H.M., Likutin, V.V., Surface chemistry of water atomised aluminium alloy powders. *Applied Surface Science*, 2002, 191: 26–43.
7. Neikov, O.D. et al., Advanced PM Aluminium Alloys Produced by New Rapid Solidification Technology. In *Proceedings of 2004 Powder Metallurgy World Congress*, Vol. 1. European Powder Metallurgy Association, 2004, pp. 230–235.
8. Faires, L.M., Inductively coupled plasma emission spectroscopy. In *ASM Handbook*, Vol. 10. ASM International Publishers, 1996, pp. 31–42.
9. Iacocca, R., Bulk and surface characterization of powders. In *ASM Handbook*, Vol. 7. ASM International Publishers, 1998, pp. 223–233.
10. Brunauer, S., Emmett, P.H., Teller, J., *Am. Chem. Soc.*, 1938, 60:309.
11. Young, D.M., Crowell, A.D., *Physical adsorption of cases*. Butterworth Publishers, London, 1962.
12. Panichkina, V.V., Uvarova, I.V., *Testing Methods of Dispersity and Specific Surface Area of Metallic Powders*. Naukova Dumka Publishers, Kiev, 1973 (in Russian).
13. Gregg, S.J., Sing, K.S.W., *Adsorption, Surface Area and Porosity*. Academic Press Publishers, 1982.
14. Lowell, S., Shields, J.E., *Powder Surface Area and Porosity*. Chapman & Hall Publishers, 1991.
15. Allen, T., *Particle Size Measurement, Vol. 2, Surface Size and Pore Size Determination*. Chapman & Hall Publishers, 1997.
16. Callis, C.F., Irani, R.R., *Miscellaneous Techniques, Particle Size: Measurements, Interpretation, and Application*. John Wiley & Sons Publishers, 1963.

17. *Method for Determination of Average Particle Size of Metal Powders Using the Fisher Subsieve Sizer, MPIF Standard 32*. MPIF Publishers, Princeton, 2003, pp 45–47.
18. Heinzer, P.J., Permeametry. In *ASM Handbook*, Vol. 7. ASM International Publishers, 1998, pp. 277–278.
19. Heinzer, P.J., Pycnometry. In *ASM Handbook*, Vol. 7. ASM International Publishers, 1998, pp. 278–280.
20. AutoPore 1V Operator's Manual, Micrometrics, 2004.
21. Naidich, Yu.V., Perevertailo, V.M., Lavrinenko, I. A., Kolesnichenko, G.A., Zhuravlev, V.S., *Surface Properties of Melts and Solids and their Usage in Material Science*. Naukova Dumka Publisher, Kiev, 1991 (in Russian).
22. Good, R.J., Mikhail, R.Sh., *Powder Technol.*, 1981 29(53).
23. Hiemenz, P.C., Rajagopalan, R., *Principles of Colloid and Surface Chemistry.* Marcel Dekker Puplisher, 1997.
24. Rootare, H.M., A Review of Mercury Porosimetry. In *Advanced Techniques in Powder Metallurgy, Vol. 5. Perspectives in Powder Metallurgy.* Plenum Press Publisher, 1970.
25. Kloubek, J., *Powder Technology*, Vol. 7. 1981, pp. 63–162.
26. Plachenov, T.G., Kolesencev, S.D., *Porosimetry*. Himiy Publishers, Leningrad, 1988 (in Russian).
27. Giesche, H., Mercury Porosimetry. In *ASM Handbook*, Vol. 7. ASM International Publishers, 1998, pp. 280–286.
28. ASTM standard D 4284, Pore Volume Distribution of Catalysts by Mercury Intrusion Porosimetry. In *Annual Book of ASTM Standards*, Vol. 5.03, ASTM International Publishers, 2003.
29. ASTM standard C 493, Bulk Density and Porosity of Granular Refractory Materials by Mercury Intrusion Porosimetry. In *Annual Book of ASTM Standards*, Vol. 15.01, ASTM International Publishers, 2003.
30. Jenike, A.W., Storage and Flow of Solids, *Bulletin of the University of Utah*, Vol. 53, No. 26. University of Utah Publisher, Salt Lake City, 1964.
31. ASTM standard D 6128, *Standard Shear Testing Method for Bulk Solids Using the Jenike Shear Cell*. ASTM Publishers, 1977.
32. Carson, J.W., Bulk properties of powders. In *ASM Handbook*, Vol. 7. ASM International Publishers, 1998, pp. 287–301.
33. Freeman, G., Production of Cobalt-Base Powders. In *ASM Handbook*, Vol. 7. ASM International Publishers, 1998, pp. 179–181.
34. Poster, A.R. (ed.), *Handbook of Metal Powders*. Reinhold Publisher, 1966.
35. Tundermann, J.H., Production of Nickel-Base Powders. In *ASM Handbook*, Vol. 7. ASM International Publishers, 1998, pp. 167–171.
36. Lux, B., Zeiler, B., Production of Tungsten and Tungsten Carbide Powders. In *ASM Handbook*, Vol. 7. ASM International Publishers, 1998, pp. 189–201.
37. Brown, R.L., Richards, J.C., *Principles of Powder Mechanics*. Pergamon Press Publisher, 1977.
38. Yokoyama, T., Fluidity of Powder. In *Powder Technology Handbook*. Marcel Dekker, Inc, 1997, pp. 413–425.
39. Henein, H., Brimacombe, J.K., Watkinson, A. P., The Modeling of Transverse Solids Motion in Rotary Kilns. *Metall. Trans. B*, 1983, 14:191–205.
40. Lumpman, S., Compressibility and Compactibility of Metal Powders, In *ASM Handbook*. ASM International Publishers, Vol. 7, 1998, pp. 302–309.